Available online at www.sciencedirect.com
SCIENCE DIRECT®
ELSEVIER
Nuclear Physics A 724 (2003) 243–273
NUCLEAR PHYSICS A
www.elsevier.com/locate/npe

Nuclear resonance fluorescence experiments on ^{204,206,207,208}Pb up to 6.75 MeV ☆

J. Enders [a,*], P. von Brentano [b], J. Eberth [b], A. Fitzler [b], C. Fransen [b], R.-D. Herzberg [b,1], H. Kaiser [a,2], L. Käubler [c], P. von Neumann-Cosel [a], N. Pietralla [b], V.Yu. Ponomarev [a,3], A. Richter [a], R. Schwengner [c], I. Wiedenhöver [b,4]

[a] *Institut für Kernphysik, Technische Universität Darmstadt, D–64289 Darmstadt, Germany*
[b] *Institut für Kernphysik, Universität zu Köln, D–50937 Köln, Germany*
[c] *Institut für Kern- und Hadronenphysik, Forschungszentrum Rossendorf, D–01314 Dresden, Germany*

Received 12 May 2003; accepted 16 May 2003

Abstract

Dipole and electric quadrupole excitations in ^{204,206,207,208}Pb have been measured up to 6.75 MeV in resonant photon scattering experiments at the superconducting Darmstadt electron linear accelerator S-DALINAC using two Euroball-Cluster detector modules. In ^{208}Pb, 14 excited states have been populated; in ^{206}Pb, the decays of 41 states have been detected. Information about 45 heretofore unknown excited states in ^{204}Pb could be measured as well as eleven known levels in ^{207}Pb. The extracted dipole strength distributions are discussed within phenomenological ("pygmy resonance") and microscopic models (quasiparticle-phonon model). A strong fragmentation and a small shift of the detected E1 strength towards higher energies is observed with the opening of the neutron shell closure.

☆ Supported by the Deutsche Forschungsgemeinschaft under contracts FOR 272/2-2, and Gr 1674/1-1, by the Bundesministerium für Bildung und Forschung under contract No. 06 OK 862 I(0), and by the Sächsisches Ministerium für Wissenschaft und Kunst under contract No. 7533-70-FZR/702.

* Corresponding author.
E-mail address: enders@ikp.tu-darmstadt.de (J. Enders).

1 Present address: Oliver Lodge Laboratory, University of Liverpool, Liverpool, UK.

2 Present address: Ingenieurbüro Fritz, Einhausen, Germany.

3 Permanent address: Bogoliubov Laboratory for Theoretical Physics, Joint Institute for Nuclear Research, Dubna, Russia.

4 Present address: Department of Physics, Florida State University, Tallahassee, FL, USA.

0375-9474/03/$ – see front matter © 2003 Published by Elsevier B.V.
doi:10.1016/S0375-9474(03)01554-9

PACS: 21.10.Re; 23.20.-g; 25.20.Dc; 27.80.+w

Keywords: NUCLEAR REACTION ^{204,206,207,208}Pb(γ, γ'), $E = 6.75$ MeV bremsstrahlung; measured $E\gamma$, $I\gamma(\theta)$. ^{204,206,207,208}Pb deduced levels, J, π, B(M1), B(E1), B(E2), pygmy resonance features. Quasiparticle-phonon model analysis

1. Introduction

The selectivity and model-independent analysis make high-resolution (γ, γ') experiments a valuable tool for the investigation of low-energy dipole modes in nuclei [1]. In recent years, progress in this field has been largely triggered by systematic studies of the orbital magnetic dipole scissors mode ([2], for recent experimental examples see, e.g., [3,4] and for reviews [5–7]). On the other hand, there is the long-standing problem to understand the nature of a concentration of E1 strength observed in many nuclei [8] in the vicinity of the particle threshold, commonly termed 'pygmy dipole resonance' (PDR). A variety of possible interpretations of the phenomenon has been proposed in—sometimes conflicting—models including hydrodynamical descriptions [9,10], neutron excess surface density oscillations [11–13], fluid-dynamical approaches [14–16] and local isospin breaking in heavy nuclei by clustering [17]. Microscopic random phase approximation (RPA) calculations in nonrelativistic [18,19] and relativistic [20–22] frameworks all predict a strong isoscalar E1 mode well below the giant dipole resonance (GDR) which may correspond to a transverse excitation mode with toroidal current distributions [23,24].

Renewed interest into this problem is partly driven by first experimental observations (see, e.g., [25,26]) of strong soft E1 modes in exotic, neutron-rich nuclei. It is an obvious question whether these modes are generated by the same mechanism in these nuclei as close to the valley of stability or whether the structural features change for extreme neutron-to-proton ratios. While most of the available data on the PDR has been derived from γ-strength functions which only provide global features, it recently has become possible [27] to study its fine structure in selected cases like Ca isotopes [28], $N = 82$ isotones [29–31] and ^{208}Pb [32] with increased sensitivity and largely reduced background. In the latter case it was possible to conclude on the nature of the PDR from the very good correspondence of the observed total E1 strength and fine structure to quasiparticle-phonon model (QPM) calculations including the coupling to complex configurations. It is found to arise from neutron surface density oscillations against an approximately isospin-saturated core [32] suggesting a similar mechanism as expected in exotic nuclei.

The present work focuses on the influence of a gradual shell opening on the low-energy dipole strength distributions by a study of the ^{208,206,204}Pb(γ, γ') reactions for excitation energies up to about 6.5 MeV. A considerably improved sensitivity compared to previous work is achieved for ^{206}Pb and ^{208}Pb, while no prior information on dipole states was available for ^{204}Pb. The energy region investigated allows an in-depth study of the interplay between one-particle–one-hole (1p–1h) and two-particle–two-hole (2p–2h) contributions to the wave functions of the populated states. Thus, the experimental results present an important test of microscopic calculations aiming at a qualitative and quantitative description of the fine structure of the dipole modes. As demonstrated, e.g., in [32], the

latter is a prerequisite for an understanding of the underlying physics. Some aspects of the present results have been discussed in [33,34].

2. Experiment and data analysis

Resonance fluorescence is an established method for the sensitive investigation of properties of low-multipolarity excitations. We refer to [1,35] and references therein for a detailed description of the technique.

2.1. Setup

The experiments have been carried out at the superconducting Darmstadt electron accelerator S-DALINAC [36]. A summary of the setup behind the superconducting injector linac and the data analysis is given, e.g., in [37]. A 3 mm tantalum disk was used for the production of the bremsstrahlung in combination with a 0.6 m long Pb collimator. The Pb target, usually sandwiched with boron disks for flux and energy calibration was located 80 cm downstream from the collimator exit. The appropriate adjustment of the target was verified using an alignment laser and taking an X-ray picture of the bremsstrahlung beam. The endpoint energy of the photon beam was checked by deflecting the electron beam with a bending magnet before and after the experiment and after adjustments involving the accelerator radio frequency controls. Two Euroball-Cluster detectors [38] with 7 HPGe crystals each were used for detecting the scattered gamma rays. The centers of the two detectors were at 132° and 94° with respect to the incoming beam direction.

The detectors were surrounded by about 30 cm of lead in each direction to shield them against diffuse gamma-ray background in the accelerator hall. The small conical opening in the shielding towards the target was covered with graded filter absorbers made of Pb and Cu (up to 3 cm each, depending on the experiment) to reduce low-energy gamma rays. The Cluster detector placed at 94° with respect to beam was equipped with BGO detectors behind the germanium crystals (back-catchers) to reduce the number of γ rays escaping due to Compton scattering or pair creation.

It is possible to enhance the full-energy peak efficiency of Cluster detectors by adding back coincident signals from detector crystals within the same module. This leads to three types of spectra used in the analysis:

- Singles spectra, i.e., spectra with no coincidences in other detector crystals can be analyzed separately. They are accumulated in multichannel memory modules.
- The so-called “add-back” spectrum contains the sum of signals from crystals in the same detector module that occur within the coincidence time window.
- In the Cluster module placed under 94° with respect to the beam, two-fold coincidences were sorted separately for the measurement of the linear polarization of the scattered radiation.

For the determination of the cross section, a full spectrum consisting of the sum of all singles spectra and the add-back spectrum was used (for each Cluster module separately).

Table 1
Experimental parameters

	^{208}Pb	^{206}Pb	^{204}Pb
Endpoint energy E_0 (MeV)	6.75(5)	6.70(5)	6.75(5)
Average electron beam current (μA)	34	27	48
Data acquisition time (h)	131	15	95
Target mass (g)	2.9555(5)	7.0656(3)	0.2292(3)
Enrichment of main component (%)	99(1)	88.3(8)	66.5(6)
Mass of ^{11}B reference target (g)	0.359(1)	0.154(1)[a]	0.154(1)[a]
	Average count rates		
Central crystal 94° (kBq)	9.6	9.3	7.6
Central crystal 132° (kBq)	9.2	8.4	7.7
Coincidences (kBq)	13.4	13.8	11.8

[a] Not used for flux calibration.

The analysis of the singles spectra allowed for a more precise analysis of the angular distribution of the gamma rays, and the two-fold coincidences from scattering in the module placed at 94° were used for parity determination.

Table 1 shows a summary of the experiments, including the electron beam parameters, data acquisition time and typical rates, and target composition. While the ^{208}Pb target was highly enriched, the main components in the other targets were significantly lower in abundance. As a consequence it was possible to assign transitions to ^{204,206,207}Pb by carefully comparing the intensities observed in the runs with the two different targets with main components ^{204}Pb and ^{206}Pb. An amount of ^{11}B was added as a reference material for the determination of the photon flux in the case of the ^{208}Pb target. For the other runs, the prominent transitions from ^{208}Pb served as a reference, and ^{11}B was only used for energy calibration.

2.2. Cross sections

2.2.1. Integrated cross section

The interaction cross section σ_f for a resonant photon scattering process from the ground state (g.s.) via an excited state into a final state with angular momentum J_f can be described by a Lorentzian

$$\sigma_f(E) = \frac{\pi}{2}\left(\frac{\hbar c}{E_\mathrm{x}}\right)^2 g\Gamma_0\Gamma_f \frac{1}{(E-E_\mathrm{x})^2+\Gamma^2/4}, \tag{1}$$

where the photon energy is denoted with E, the maximum of the resonance is at E_x, and the width of the state is Γ. The quantities Γ_0 and Γ_f denote the partial widths for the decay into the g.s. and into an arbitrary final state (often also the g.s.), respectively. The statistical factor $g = (2J+1)/(2J_0+1)$ with the angular momenta J and J_0 of the excited state and the g.s., respectively, takes into account the degeneracy of the magnetic quantum number.

For particle-bound excitations, the typical detector resolution of several keV is much larger than the intrinsic line width so that the observed signal corresponds to an energy-integrated cross section

$$I_f = \int \mathrm{d}E\, \sigma_f(E) = \frac{\pi}{2} \Gamma_f \sigma_{\mathrm{abs}}^{\max}, \tag{2}$$

with $\sigma_{\mathrm{abs}}^{\max} := 2\pi(\hbar c/E_{\mathrm{x}})^2 g\Gamma_0/\Gamma$. Experimentally, the cross section is determined from the number of detected events A_f. This number is proportional to the quantity

$$A_f \propto \int_{E_{\mathrm{x}}-\delta E}^{E_{\mathrm{x}}+\delta E} \mathrm{d}E\, \sigma_f(E)\eta(E), \tag{3}$$

where $\eta(E)$ denotes an attenuation factor for the photon flux containing both nonresonant and resonant contributions.

2.2.2. Self-absorption effects

The attenuation factor depends on the target geometry. While the nonresonant attenuation can be extracted by measuring simultaneously a well-known material sandwiched or mixed with the target, the resonant self-absorption effects need to be corrected numerically, especially for thick targets and strong excitations. In this case, the photon flux in the vicinity of excitations gets attenuated due to the resonant photon interaction cross section $\sigma_{\mathrm{abs}}^{\max} \cdot \psi$ and nonresonant contributions κ_{NR} as a function of the target thickness. The function ψ denotes the line shape which depends on the photon energy $E = \Gamma x/2 + E_{\mathrm{x}}$, the room temperature, and the properties of the target material. The detected signal therefore amounts to

$$A_f \propto \int \mathrm{d}x\, \frac{1 - \exp[-d(\sigma_{\mathrm{abs}}^{\max}\psi(x) + \kappa_{\mathrm{NR}})]}{\sigma_{\mathrm{abs}}^{\max}\psi(x) + \kappa_{\mathrm{NR}}} \psi(x) \tag{4}$$

with target thickness d. (For a detailed discussion, see, e.g., [35].) This equation has to be solved numerically both for reference and the target material. In the present analysis, we have expanded the exponential function into a power series (see also [39]) up to 5th order

$$A_f \propto \sum_{k=0}^{5} \sum_{j \leqslant k} \frac{(-)^k}{(k+1)!} d^{k+1} \binom{k}{j} \left(\sigma_{\mathrm{abs}}^{\max}\right)^{k-j+1} \kappa_{\mathrm{NR}}^{j} \int \mathrm{d}x\, \psi^{k-j+1}. \tag{5}$$

The calculation of the integral $\int \mathrm{d}x\, \psi^{k-j+1}$ is performed numerically to an accuracy of about 2%. This affects correction terms $(k - j + 1) > 1$ only so that this contribution can be neglected against typical statistical and systematic uncertainties.

2.2.3. Transition widths and strengths

If all partial decay branches are known, one can extract the transition width from the measured cross section. From this the reduced transition strength $B(\mathrm{E/M}\lambda)$ can be deduced for a given multipole order λ. Especially for odd-mass nuclei it is convenient to use a reduced transition width for the decay into the g.s.

$$g\Gamma_0^{\mathrm{red}} = g\frac{\Gamma_0}{E_{\mathrm{x}}^3} \tag{6}$$

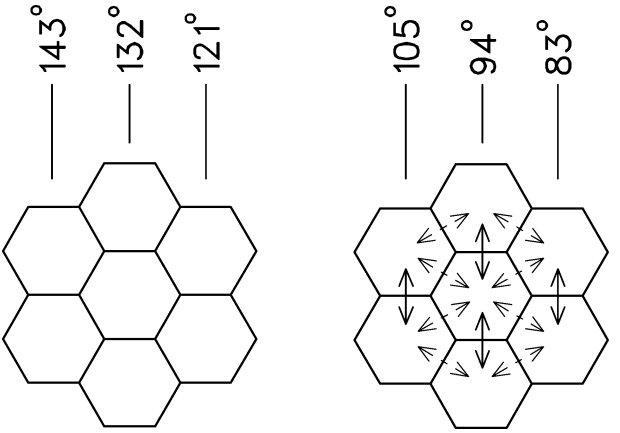

Fig. 1. Schematic drawing of the two Cluster detectors as seen from the target (incoming photon beam from the left side). Two, respectively, three individual crystals are located at one common polar scattering angle so that the singles data of these crystals can be summed to yield a precise six-point angular distribution. For the Cluster detector placed at 94° with respect to the incoming beam a measurement of the linear polarization of the scattered photons was performed. Two-fold events at 90° with respect to the reaction plane (full arrows) were compared with events at 30° and 150°, respectively (dashed arrows).

instead of the dipole transition strength. This quantity is related to the $B(\mathrm{E/M1})$ value via

$$\frac{g\Gamma_0^{\mathrm{red}}}{(\mathrm{meV/MeV^3})} = 1.047\frac{B(\mathrm{E1}\uparrow}{(10^{-3}\,e^2\,\mathrm{fm}^2)}, \tag{7}$$

$$\frac{g\Gamma_0^{\mathrm{red}}}{(\mathrm{meV/MeV^3})} = 11.57\frac{B(\mathrm{M1}\uparrow}{(\mu_N^2)}. \tag{8}$$

Note that these relations neglect multipole mixing, especially for the case of M1/E2 mixing.

2.3. Angular distributions

The angular distribution of the resonantly scattered photons depends for an unpolarized photon beam on the angular momenta of the g.s., the intermediate, and the final state, the multipole order λ and, if applicable, the mixing parameter δ. For even–even nuclei and transitions into the g.s., the angular distributions for dipole and quadrupole transitions have characteristic minima at 90° and 127°, respectively. In the present setup, the detectors have been located close to these angles. The composite Cluster modules allow the extraction of angular distributions beyond such a simple two-point measurement from an analysis of the singles spectra. Fig. 1 shows a schematic drawing of the two Cluster detectors as seen from the target position. (The incoming beam would be from the left.) Groups of two or three detectors are located at a specific scattering angle with respect to the incoming beam so that the measurement of six points of an angular distribution is possible. This enhanced sensitivity can be used, e.g., for the determination of multipole mixing parameters in odd-mass nuclei.

2.4. Parity determination

For $0^+ \to 1^\pm \to 0^+$ transitions, i.e., in particular for dipole excitations in even–even nuclei, it is possible to determine the parity of the intermediate state from a measurement of the linear polarization of the scattered radiation close to 90°. The polarization can be determined from a double-scattering experiment. The composite Cluster modules allow one to analyze the Compton scattering between detector crystals at angles of 30°, 150° and 90° with respect to the reaction plane as indicated by the arrows in Fig. 1. Cluster detectors have a low polarization sensitivity due to their hexagonal geometry compared to dedicated detectors [40]. This effect is to some extent compensated by a high coincidence efficiency [41] so that a polarization measurement for the strongest excitations has been shown to be feasible [30]. A considerably higher sensitivity to the multipole character of dipole excitations in photon scattering processes can only be achieved by using intense polarized γ-ray beams in the entrance channel as was recently demonstrated [42]. Application of this technique to the semi-magic nuclei ^{138}Ba [43] and ^{88}Sr [44] supports the interpretation that by far most of the dipole excitations close to the particle separation energy have electric character.

3. Results and discussion

3.1. The $^{208}Pb(\gamma, \gamma')$ reaction

The summed photon scattering spectrum of the Cluster detector placed at 132° with respect to the incoming beam—containing the sum of the singles spectra as well as the add-back spectrum—is shown in Fig. 2. The displayed energy range is 4 to 7 MeV. The spectrum shows few rather strong excitations which clearly stand out from the background. One observes also single and double-escape peaks as well as transitions from the reference material ^{11}B. Transitions into the g.s. of ^{208}Pb are indicated by arrows. Decay into excited states should play a minor role because of the reduced level density at low E_x in a doubly magic nucleus.

Fig. 3 shows the two-point angular distribution ratio of the two Cluster detectors which is sufficient for disentangling dipole and quadrupole excitations. The dashed lines in Fig. 3 indicate the expected ratios for dipole and quadrupole excitations including an averaging over the finite detector opening angle. One recognizes that the measured angular distributions exhibit a tendency to be more isotropic than expected. Neither the divergence of the incoming photon beam nor the positioning of the detectors can account for the observed result.

In addition to the analysis using the summed spectra of the Cluster detectors, the angular distribution for 6 scattering angles was deduced from the analysis of the singles spectra. The results for the transitions in ^{208}Pb are shown in Fig. 4. The solid and dashed lines show the theoretical distributions for dipole and quadrupole transitions, respectively.

From the two-fold coincidences in the Cluster detector module at 94° experimental asymmetries have been extracted. Results are shown in Fig. 5. Only for the strongest transitions are parity assignments unambiguous. The results are consistent with the

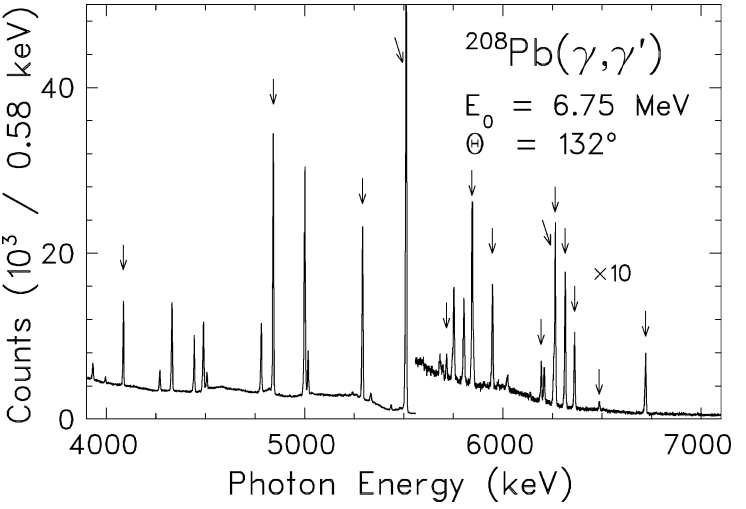

Fig. 2. Spectrum of the ^{208}Pb(γ, γ') reaction taken with the Euroball-Cluster detector at 132° at an endpoint energy of 6.75 MeV. Arrows mark transitions into the ground state of ^{208}Pb.

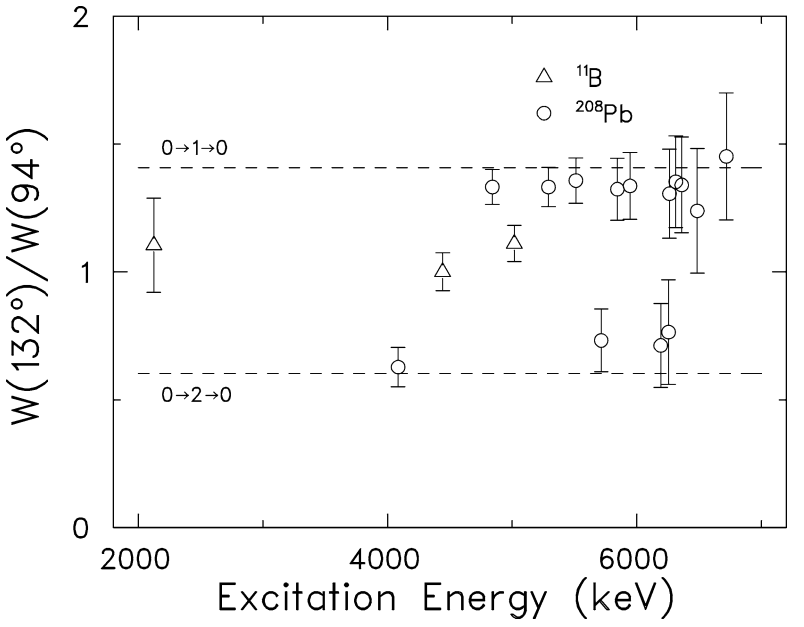

Fig. 3. Angular distribution ratio $W(132°)/W(90°)$ of transitions in ^{208}Pb for the full Cluster detectors. The dashed lines indicate the theoretical values for pure dipole and quadrupole transitions, respectively, after correction for the finite opening angle of the detectors. The values for ^{208}Pb (open circles) have been normalized to the calibration material ^{11}B (open triangles).

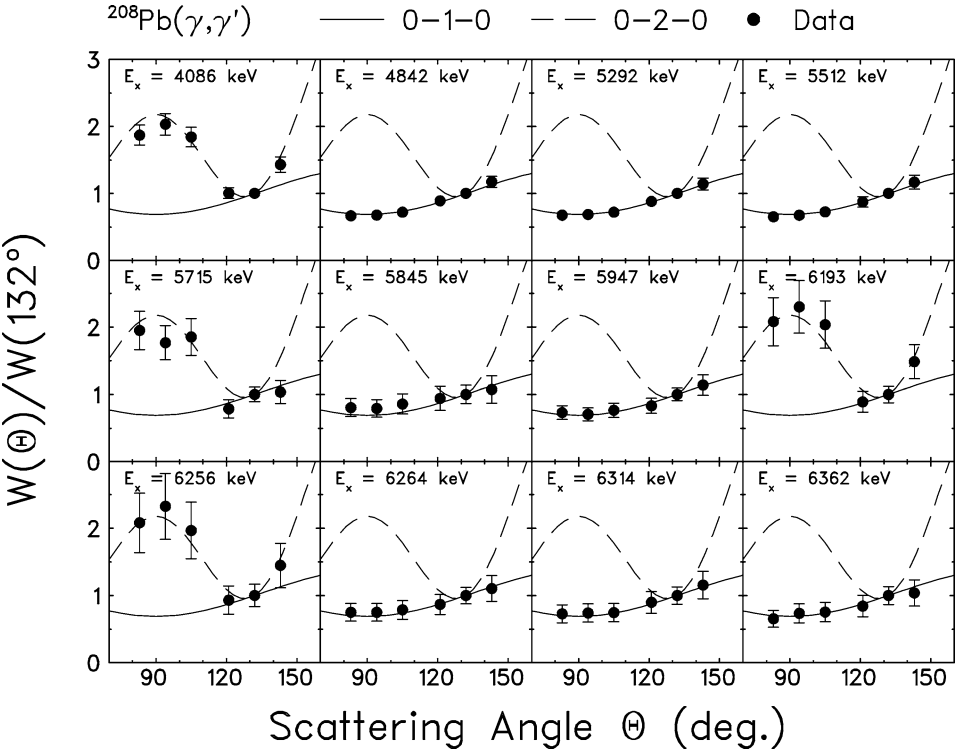

Fig. 4. Angular distribution ratios $W(\Theta)/W(132^\circ)$ of transitions into the ground state of ^{208}Pb for the six effective scattering angles of the individual crystals of the two Cluster detectors. The distributions have been normalized to the value at $\Theta = 132^\circ$. The full and dashed lines indicate the theoretical distributions for dipole and quadrupole excitations, respectively.

literature [45]. Parity assignments have not been possible for the experiments with the ^{204,206}Pb targets.

Table 2 lists the deduced values for excitation energy, spin and parity, branching ratio into the g.s., the quantity Γ_0^2/Γ which is proportional to the integrated cross section, the excitation strength, and lifetimes of the detected excitations. For the states at 4842 keV and 5292 keV literature values [45,46] for the branching ratios were used for the analysis alternatively to $\Gamma_0/\Gamma = 1$ from the present experiment. The deduced quantities include self-absorption corrections which can be as large as 23% for the 5512 keV excitation.

A comparison of the results obtained in the present experiment with previous investigations is shown in Table 3. In the studied energy interval, three known states have been measured in photon scattering for the first time. In agreement with the adopted values [45,52] and in conflict with Ref. [49] we identify negative parity for the state at 4842 keV. No decays into excited states of ^{208}Pb have been observed. Due to the nonresonant background an upper limit for decay branches to low-lying states is found to be about 15–20%. For the 5716 keV state we assign $J^\pi = 2^+$. The M1 excitation strength of the 5845 keV state is in agreement with [52]; this strength is somewhat larger than the

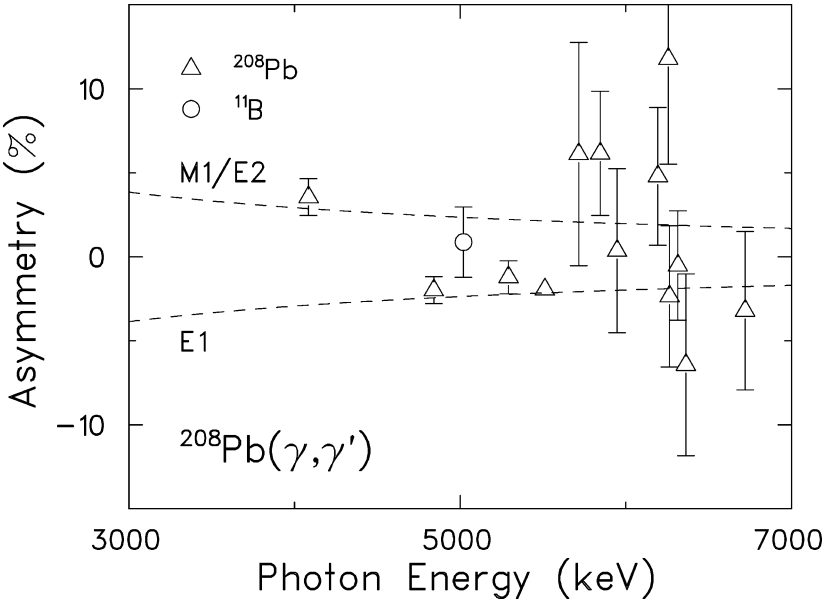

Fig. 5. Asymmetry of the radiation scattered in the Cluster detector placed under 94° with respect to the incoming beam for transitions into the ground state of ^{208}Pb (open triangles). The isotropic distribution of a transition in ^{11}B is shown for comparison (open circle). The dashed lines indicate an extrapolation of the expected asymmetry of the Cluster detector for a detection threshold of 150 keV [41]. Magnetic dipole and electric quadrupole transitions have positive, electric dipole transitions negative asymmetry.

Table 2
Results of the ^{208}Pb(γ, γ') experiment. The excitation energies E_x, the angular momentum and parity values J^π, the branching ratio Γ_0/Γ, the ratio Γ_0^2/Γ, the reduced transition strength $B(\sigma\lambda)$, and the life time τ are given

E_x (keV)	J^π ($\hbar$)	Γ_0/Γ	Γ_0^2/Γ (eV)	$B(\sigma\lambda)\uparrow$ ([a])	τ (fs)
4085.5(2)	2^+	1.0	0.45(3)	2434(168)	1.47(10)
4841.7(3)	1^-	1.0	4.78(31)	121(8)	0.14(1)
		0.85[b]	4.69(30)	139(9)	0.10(1)
5292.3(3)	1^-	1.0	6.31(43)	122(8)	0.10(1)
		0.78[b]	6.13(42)	152(10)	0.065(4)
5512.1(3)	1^-	1.0	28.3(21)	484(36)	0.023(2)
5715.5(4)	2^+	1.0	0.13(2)	127(17)	5.25(40)
5844.9(4)	1^+	1.0	1.67(16)	2.17(21)	0.39(5)
5947.0(4)	1^-	1.0	1.13(11)	15.4(16)	0.58(8)
6193.1(4)	2^+	1.0	0.57(7)	388(48)	1.15(11)
6255.6(4)	2^+	1.0	0.50(7)	323(47)	1.32(13)
6263.8(4)	1^-	1.0	4.17(54)	48.6(63)	0.16(2)
6313.9(4)	1^-	1.0	3.34(52)	38.0(59)	0.20(4)
6361.6(4)	1^-	1.0	2.05(37)	22.8(41)	0.32(5)
6486.4(5)	1^-	1.0	0.29(8)	3.0(10)	2.29(47)
6719.7(5)	1^-	1.0	4.37(248)	41.3(235)	0.15(9)

[a] E1 strength in $10^{-3}\ e^2\ \mathrm{fm}^2$, M1 strength in μ_N^2, E2 strength in $e^2\ \mathrm{fm}^4$.

[b] Branching ratio from [45].

Table 3
Comparison of nuclear resonance fluorescence experiments on ^{208}Pb

E_x (keV)	Γ_0^2/Γ^a (eV)	Γ_0^2/Γ^b (eV)	Γ_0^2/Γ^c (eV)	Γ_0^2/Γ^d (eV)	Γ_0^2/Γ^e (eV)	Γ_0^2/Γ^f (eV)	Γ_0^2/Γ^g (eV)	Γ_0^2/Γ^h (eV)
4086	0.45(3)	0.68(15)	0.51(20)	0.49(5)				
4842	4.78(31)	5.0(8)	6.3(22)	5.1(8)	6(2)		4.7(9)	6.9(14)
5292	6.31(43)	5.1(8)	8.6(30)		7(2)	5.2(15)		7.0(14)
5512	28.3(21)	22.3(34)	28(10)		18(3)	17.7(48)		21.4(22)
5716	0.13(2)							
5845	1.67(16)						1.2(4)	
5947	1.13(11)	1.0(3)						
6193	0.57(7)							
6256	0.50(7)							
6264	4.17(54)	2.6(5)	4.1(18)			3.0(11)		
6314	3.34(52)	3.2(6)	1.0					
6362	2.05(37)	1.6(4)	0.5					
6486	0.29(8)							
6720	> 4.37	7.6(15)	15(6)		13(3)	6.9(20)		13.0(16)

[a] This paper.
[b] Ref. [46].
[c] Ref. [47].
[d] Refs. [48,49].
[e] Ref. [50].
[f] Ref. [51].
[g] Ref. [52].
[h] Ref. [53].

results from (e,e′) and the discrepancy persists [54,55]. The 1^- state at 6720 keV is very close to the endpoint of the photon spectrum. The extracted excitation strength is therefore a lower limit only. A more elaborate discussion of the results on a state-by-state basis is given elsewhere [56].

3.2. The $^{206}Pb(\gamma,\gamma')$ reaction

The summed photon scattering spectrum of the ^{206}Pb(γ,γ') reaction of the Cluster detector at 132° is shown in Fig. 6 for the energy range of 4 to 7 MeV. The spectrum shows a rich structure, but we stress that the enrichment of the isotope ^{206}Pb was only 88% so that transitions from ^{207,208}Pb are visible, too. Arrows identify transitions into the g.s. of ^{206}Pb, and the brackets indicate decay branches into the 2_1^+ state in ^{206}Pb at 803 keV, concluded from the transition energies.

Fig. 7 shows the two-point angular distribution ratios with circles indicating transitions in ^{206}Pb and triangles labeling transitions from the ^{208}Pb component in the target. Full circles denote transitions to the first 2^+ state in ^{206}Pb. Decay branches to excited states are identified by energy differences only. The angular distributions of transitions into excited final states with $J \neq 0$ depend on the multipole mixing parameter and do not need to coincide with the dashed lines that indicate once more the theoretical values for decays into the g.s. We omit here examples for angular distributions from the singles spectra. They

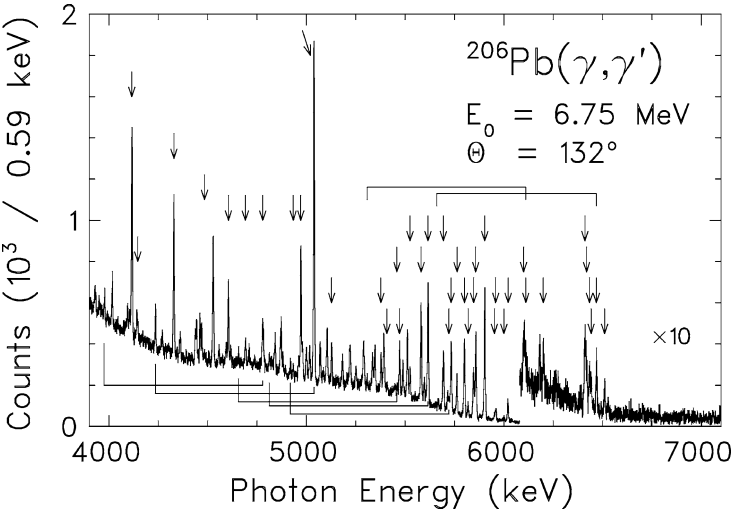

Fig. 6. Spectrum of the ^{206}Pb(γ, γ') reaction taken with the Euroball-Cluster detector at 132° at an endpoint energy of 6.70 MeV. Arrows mark transitions into the ground state of ^{206}Pb; brackets show branchings into the 2_1^+ state in ^{206}Pb.

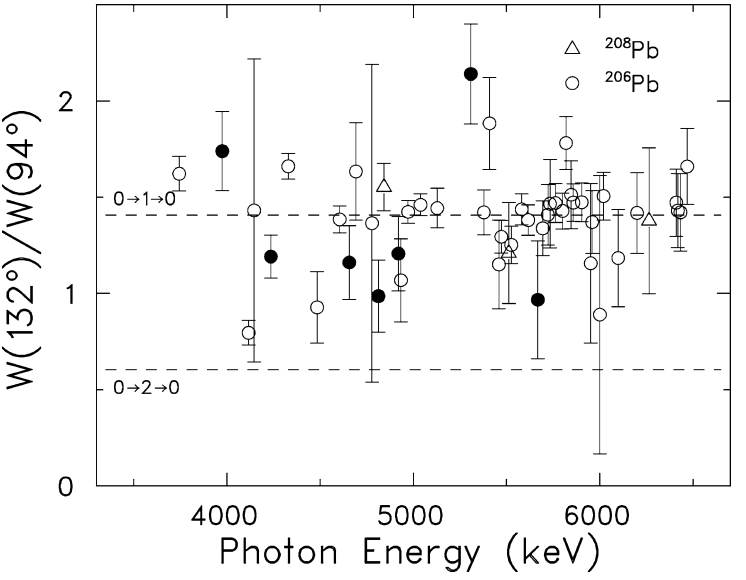

Fig. 7. Angular distribution ratio $W(132°)/W(90°)$ of transitions in ^{206}Pb for the full Cluster detectors. The dashed lines indicate the theoretical values for pure dipole and quadrupole transitions, respectively, after correction for the finite opening angle of the detectors. Circles indicate transitions into the ground state of ^{206}Pb (open symbols) and into the 2_1^+ state of ^{206}Pb (full symbols). The values for ^{206}Pb have been normalized to the transitions in ^{208}Pb (triangles).

are shown elsewhere [56]. The polarization analysis did not lead to statistically significant results.

Weak transitions detected in the spectrum were assigned to ^{206}Pb in combination with the analysis of the ^{204}Pb(γ,γ') experiment (see below). The combination of the two measurements allowed the transitions from ^{204,206,207}Pb to be disentangled. A group of previously unknown transitions around 6.4 MeV, however, was detected in both measurements, and the intensity ratios suggest that these transitions are from ^{207}Pb. If this assumption was true, previous experiments (e.g., [46]) with highly enriched ^{207}Pb targets should have been able to detect these excitations. Thus it is assumed that this group of transitions exists at basically identical energies both in ^{204}Pb and ^{206}Pb. For ^{206}Pb the extracted excitation strengths are of the order of the sensitivity limit of previous experiments. Table 4 summarizes the results. For excitations whose multipole order could neither be extracted from the angular distribution nor from the literature [57], a 0–1–0 cascade was assumed. Transition strengths are listed in units of the E1 strength where no parity assignment was possible. Self-absorption corrections have been included.

Table 4
Results of the ^{206}Pb(γ,γ') experiment. The listed quantities are explained in Table 2. For excitations where an unambiguous assignment of the multipolarity was not possible, the transition strength is given as E1 strength

E_x (keV)	J^π ($\hbar$)	Γ_0/Γ	Γ_0^2/Γ (eV)	$B(\sigma\lambda)\uparrow$ ([a])	τ (fs)
3743.7(7)	1^-	1.0	0.09(1)	4.9(6)	7.36(87)
4116.0(7)	2^+	1.0	0.29(3)	1506(158)	2.29(24)
4145.9(8)	$1^\pm$	1.0	0.03(2)	1.0(7)	26.3(185)
4328.6(5)	1^-	1.0	0.33(4)	11.7(12)	1.99(21)
4483.5(5)	2^+	1.0	0.02(1)	83(15)	27.1(50)
4604.6(4)	1^-	1.0	0.25(3)	7.3(8)	2.66(29)
4691.4(4)[b]	$1^\pm$	1.0	0.08(2)	2.1(4)	8.6(19)
4778.6(10)[c]	$1^\pm$	$0.75^{+0.25}_{-0.45}$[d]	0.20(14)	7.1(48)	1.83(125)
4933.3(5)	$(1^\pm, 2^+)$	1.0	0.04(1)	0.9(2)	17.3(38)
4972.0(3)	1^-	1.0	0.70(7)	16.3(17)	0.94(10)
5038.5(2)	1^-	$0.94^{+0.06}_{-0.21}$	2.12(21)	50.6(51)	0.27(3)
5128.0(3)	$1^\pm$	1.0	0.23(3)	4.9(6)	2.87(36)
5378.1(3)	$1^\pm$	1.0	0.28(4)	5.1(7)	2.38(32)
5408.4(5)	$(1^\pm)$	1.0	0.09(2)	1.6(3)	7.6(17)
5459.1(6)	$(1^\pm, 2^+)$	$0.51^{+0.19}_{-0.11}$	0.09(2)	3.0(7)	1.97(44)
5471.8(3)	$1^{(-)}$	1.0	0.58(7)	10.2(12)	1.13(13)
5525.1(3)	$1^\pm$	1.0	0.40(5)	6.8(8)	1.64(20)
5581.1(3)	1^-	1.0[e]	1.47(17)	24.2(27)	0.45(6)
5616.1(3)[f]	$1^{(-)}$	$0.94^{+0.06}_{-0.24}$	2.02(23)	34.8(39)	0.29(3)
5694.1(4)	1^-	1.0	0.95(14)	14.8(22)	0.69(10)
5722.1(6)	$1^\pm$	$0.67^{+0.25}_{-0.15}$	0.19(3)	4.4(7)	1.52(25)
5733.3(4)	1^-	1.0	1.44(32)	21.9(48)	0.46(10)
5762.6(4)	1^-	1.0	0.68(9)	10.2(13)	0.96(12)
5800.5(4)	1^+	1.0	1.68(20)	2.23(27)	0.39(5)
5819.1(5)	1^-	1.0	0.25(4)	3.7(6)	2.6(4)
5846.5(4)	1^-	1.0	1.15(21)	16.4(29)	0.57(10)

(*continued*)

Table 4 (*Continued*)

E_x (keV)	J^π ($\hbar$)	Γ_0/Γ	Γ_0^2/Γ (eV)	$B(\sigma\lambda)\uparrow$ ([a])	τ (fs)
5858.2(4)	1^-	1.0	2.17(27)	30.9(38)	0.30(4)
5903.6(4)	1^-	1.0	3.48(44)	48.5(61)	0.19(3)
5951.8(12)	$(1^\pm, 2^+)$	1.0	0.13(5)	1.8(7)	5.0(18)
5959.2(5)	$1^\pm$	1.0	0.34(6)	4.7(8)	1.9(3)
6000.4(7)[g]	$(1^\pm, 2^+)$	1.0	0.09(5)	1.2(7)	7.4(42)
6021.5(5)	$1^\pm$	1.0	0.66(9)	8.6(12)	1.00(14)
6100.2(15)	$(1^\pm, 2^+)$	1.0	0.32(7)	4.0(9)	2.06(47)
6110.7(10)	$(1^\pm, 2^+)$	$0.35^{+0.11}_{-0.12}$	0.12(4)	4.3(14)	0.67(25)
6200.4(7)	$1^\pm$	1.0	0.21(4)	2.5(5)	3.14(64)
6410.5(6)[h]	$1^\pm$	1.0	0.65(15)	7.1(17)	1.01(24)
6418.8(8)[h]	$1^\pm$	1.0[i]	0.40(10)	4.3(11)	1.65(42)
6433.7(7)	$1^\pm$	1.0	0.35(10)	3.7(10)	1.90(54)
6442.4(9)	$(1^\pm)$	1.0	0.22(9)	2.4(10)	2.96(123)
6469.2(8)[h]	$1^\pm$	$0.82^{+0.18}_{-0.41}$[j]	0.46(42)	5.9(54)	0.97(88)
6510.6(10)	1^-	1.0	0.24(20)	2.5(21)	2.8(25)

[a] E1 strength in $10^{-3}\ e^2\ \mathrm{fm}^2$, M1 strength in μ_N^2, E2 strength in $e^2\ \mathrm{fm}^4$.

[b] Assignment to ^{206}Pb unclear; transition coincides with a single-escape peak in the experiment with ^{204}Pb as main component.

[c] Contributions from single- and double-escape peaks ($\sim 50\%$) subtracted.

[d] Transition into the ground state coincides with a possible branch of the state at 5581 keV.

[e] Possible branch to the 2_1^+ state coincides with the transition at 4779 keV.

[f] Transition into the ground state coincides with a possible branch of the state at 6419 keV.

[g] Contribution from a single-escape peak subtracted ($\sim 40\%$).

[h] Assignment to ^{206}Pb unclear; transition coincides with a transition from the measurement with main component ^{204}Pb.

[i] Possible branch to the first excited state coincides with the strong transition at 5616 keV.

[j] Branch to the first excited state coincides with the single-escape peak of a transition in ^{207}Pb; contribution subtracted ($\sim 50\%$).

Comparing the present results to previous photon scattering work, one finds generally good agreement, see Table 5. For the 4484 keV level, known previously from (n,n$'\gamma$) and (p,t) reactions [58,59], the assignment $J^\pi = 2^+$ was possible. The detected peak at 4779 keV was difficult to interpret. There is a decay branch to the 2_1^+ state associated with a level at that energy, while the 4779 keV transition can also be viewed as a branch of the 5581 keV level. The peak also coincides with single and double-escape peaks. Combining our findings with the (n,n$'\gamma$) results of Ref. [58], we assume a transition into the g.s. In conflict with the findings of [58], no decay branch to the 1704 keV level was observed for this state. Electron scattering experiments [60] report an E2 excitation close to the 5128 keV level. However, on the basis of the measured angular distribution as well as the extracted transition width an assignment $J^\pi = 2^+$ is unlikely. Previously reported decay branches of states at 5694 keV, 5733 keV, and 5819 keV to the 2_2^+ state could not be detected, but their transition strengths are again around the present detection limit. The states at 6100 keV and 6111 keV are close to a known E2 excitation detected in (e,e$'$) at 6103(10) keV [60]. While the measured angular distribution in the present experiment is not conclusive, the extracted transition width is comparable with the electron scattering

Table 5
Comparison of results of nuclear resonance fluorescence experiments on ^{206}Pb. Only the previously measured transitions that are listed in Table 4 are given

E_x (keV)	Γ_0^2/Γ^a (eV)	Γ_0^2/Γ^b (eV)	Γ_0^2/Γ^c (eV)	Γ_0^2/Γ^d (eV)
3744	0.09(1)			0.13(2)
4116	0.29(3)	0.58(15)		0.30(6)
4329	0.33(4)	0.48(11)		0.90(9)
4605	0.25(3)	0.58(16)		0.23(3)
4972	0.70(7)	0.95(23)	0.8(3)	0.8(2)
5039	2.12(21)	2.6(4)	1.6(6)	2.3(5)
5472	0.58(7)	0.7(2)		
5581	1.47(17)	1.7(3)	0.5[e]	
5616	2.02(23)	1.8(4)	1.0[e]	
5694	0.95(14)	0.8(2)	0.5[e]	
5733	1.44(32)	1.3(3)		
5763	0.68(9)	0.9(2)		
5801	1.68(20)	1.1(3)	1.0[e]	
5819	0.25(4)	0.5(2)		
5847	1.15(21)	1.1(2)	3.0[e]	
5858	2.17(27)	2.0(4)		
5904	3.48(44)	3.0(6)		
6511	0.24(20)	1.9(4)		

[a] This paper.
[b] Ref. [46].
[c] Ref. [47].
[d] Ref. [48].
[e] Estimated uncertainty in excess of 50%.

result. The excitation at 6511 keV is much weaker than reported previously [46]. This is most likely due to a transition of a higher-lying state not excited in the present experiment to a low-lying excited state that coincides with the energy of the excitation at 6511 keV. Further details and a more elaborate discussion on single levels are given elsewhere [56].

3.3. *The $^{204}Pb(\gamma,\gamma')$ reaction*

Fig. 8 shows the photon scattering spectrum in the range 4–7 MeV for the experiment with the enriched ^{204}Pb target. Transitions into the g.s. are labeled with arrows; brackets indicate decay branches into the 2_1^+ state at 899 keV. Aside from the rich fine structure that can be attributed to ^{204}Pb one observes transitions from ^{206,207,208}Pb due to the relatively low enrichment of the target material. Transitions from ^{11}B—used for energy calibration purposes—are visible as well. The photon flux was normalized to prominent transitions from ^{208}Pb.

The two-point angular distribution ratios are shown in Fig. 9, and Fig. 10 displays selected examples of the angular distributions as derived from the singles spectra for strong excitations below 5.7 MeV. Circles in Fig. 9 denote transitions in ^{204}Pb—open symbols for transitions into the g.s., full symbols for transitions into the 2_1^+—and triangles transitions in ^{208}Pb used for normalization. Most observed angular distributions above 4.5 MeV are very close to the theoretical expectation for dipole excitations. Parity determination was not possible due to the low statistics.

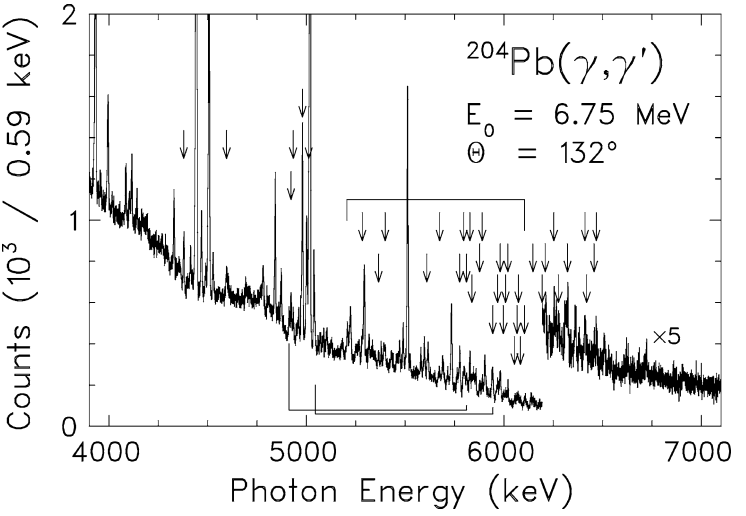

Fig. 8. Spectrum of the ^{204}Pb(γ, γ') reaction taken with the Euroball-Cluster detector at 132° at an endpoint energy of 6.75 MeV. Arrows mark transitions into the ground state of ^{204}Pb; brackets show branchings into the 2_1^+ state in ^{204}Pb.

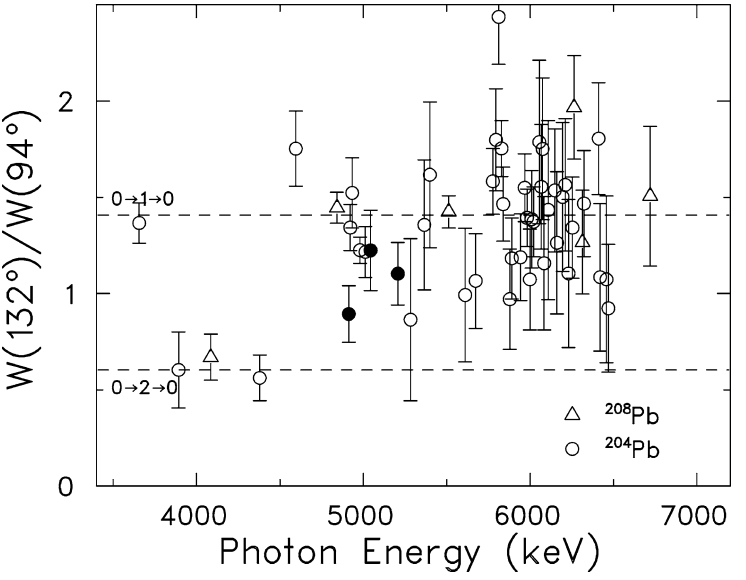

Fig. 9. Angular distribution ratio $W(132°)/W(90°)$ of transitions in ^{204}Pb for the full Cluster detectors. The dashed lines indicate the theoretical values for pure dipole and quadrupole transitions, respectively, after correction for the finite opening angle of the detectors. Circles indicate transitions into the ground state of ^{204}Pb (open symbols) and into the 2_1^+ state of ^{204}Pb (full symbols). The values for ^{204}Pb have been normalized to the transitions in ^{208}Pb (triangles).

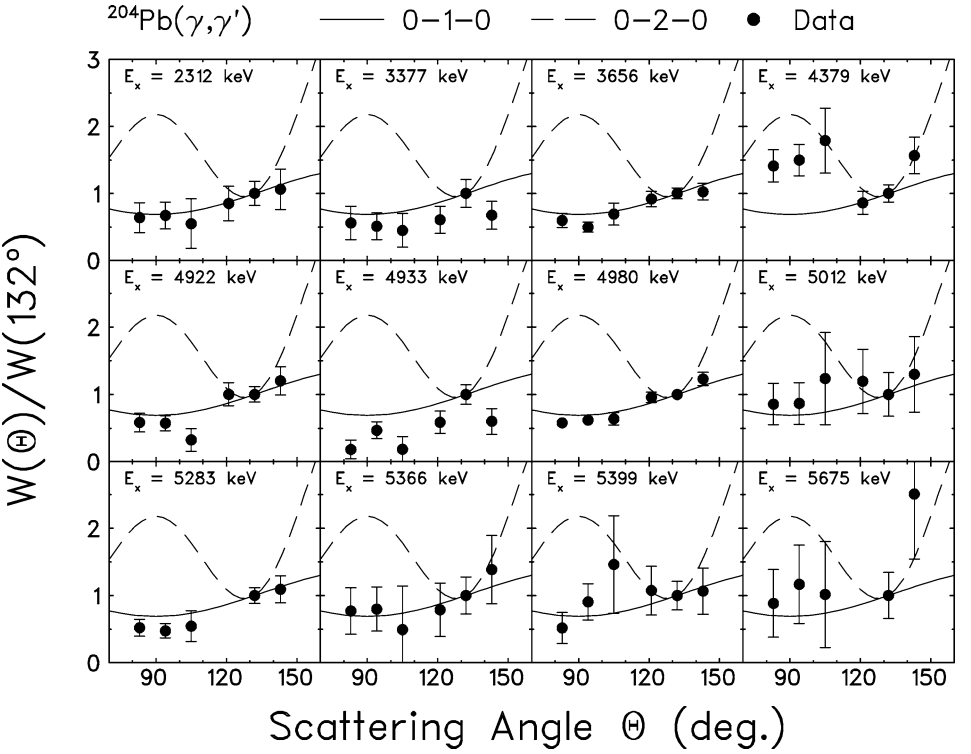

Fig. 10. Angular distribution ratios $W(\Theta)/W(132°)$ of selected low-lying transitions into the ground state of ^{206}Pb for the six effective scattering angles of the individual crystals of the two Cluster detectors. The distributions have been normalized to the value at $\Theta = 132°$. The full and dashed lines indicate the theoretical distributions for dipole and quadrupole excitations, respectively.

As discussed above, a combined analysis of the experiments with main components ^{206}Pb and ^{204}Pb resulted in a rather clear assignment of weak transitions to the different nuclei. The results for ^{204}Pb are given in Table 6. None of the detected transitions had been observed in a previous experiment. Self-absorption effects are negligible.

3.4. The $^{207}Pb(\gamma,\gamma')$ reaction

From the two experiments with the main components ^{206}Pb and ^{204}Pb it was possible to extract reduced transition widths also for the odd-mass nucleus ^{207}Pb. Due to the low enrichment in the two targets and the complex spectra from ^{204,206,208}Pb the sensitivity for this isotope in the present experiment is clearly lower.

For nuclei with odd mass number the angular distribution is nearly isotropic for most values of the multipole mixing parameter δ so that the identification of the angular momentum of excited states is hardly feasible. Determining six points of the angular distribution from the singles spectra in principle improves this situation. Fig. 11 shows distributions for transitions in ^{207}Pb extracted from the measurement with a mixed target with main component ^{206}Pb. The theoretical distributions are for an intermediate state with

Table 6
Results of the ^{204}Pb(γ, γ') experiment. The listed quantities are explained in Table 2. For excitations where an unambiguous assignment of the multipolarity was not possible, the transition strength is given as E1 strength

E_x (keV)	J^π ($\hbar$)	Γ_0/Γ	Γ_0^2/Γ (eV)	$B(\sigma\lambda)\uparrow$ ([a])	τ (fs)
2311.6(6)	$1^\pm$	1.0	0.02(1)	5.4(10)	28(6)
3377.4(7)	$1^\pm$	1.0	0.03(2)	2.5(4)	19(4)
3656.3(3)	$1^\pm$	1.0	0.12(1)	7.2(8)	5.4(5)
3893.2(6)	2^+	1.0	0.03(1)	182(29)	25(4)
4379.0(2)	2^+	1.0	0.11(1)	439(46)	5.8(6)
4596.1(8)	$1^\pm$	1.0	0.09(2)	2.6(5)	7.6(16)
4922.0(3)[b]	$1^\pm$	1.0	0.18(4)	4.4(10)	3.6(8)
4933.1(3)[c]	$1^\pm$	1.0	0.09(4)	2.1(13)	7.7(39)
4980.3(2)[d]	$1^\pm$	1.0	0.79(26)	18.3(61)	0.84(28)
5011.9(3)	$1^\pm$	1.0	0.54(6)	12.3(14)	1.22(14)
5283.1(5)[e]	$(1^\pm, 2^+)$	1.0	0.16(12)	3.2(24)	4.0(30)
5365.8(6)[e]	$(1^\pm, 2^+)$	1.0	0.08(6)	1.4(12)	8.7(73)
5398.7(5)	$1^\pm$	1.0[f]	0.16(4)	3.0(8)	4.0(11)
5610.2(9)	$(1^\pm, 2^+)$	1.0[g]	0.15(4)	2.5(7)	4.4(12)
5674.9(12)	$(1^\pm, 2^+)$	1.0	0.22(4)	3.5(7)	3.0(6)
5776.6(4)	$1^\pm$	1.0	0.91(13)	13.6(19)	0.72(10)
5795.5(6)	$1^\pm$	1.0	0.33(7)	4.8(10)	2.0(4)
5811.3(5)[h]	$1^\pm$	$0.36^{+0.23}_{-0.16}$	0.17(14)	6.8(59)	0.51(45)
5828.3(3)	$1^\pm$	1.0	0.80(10)	11.5(14)	0.83(10)
5838.4(4)	$1^\pm$	1.0	0.37(6)	5.3(8)	1.8(3)
5877.8(6)	$(1^\pm, 2^+)$	1.0	0.28(6)	4.0(8)	2.3(5)
5890.6(5)	$(1^\pm, 2^+)$	1.0	0.35(6)	4.9(8)	1.9(3)
5943.8(12)[i]	$(1^\pm, 2^+)$	$0.74^{+0.26}_{-0.20}$	0.82(30)	15.1(55)	0.44(30)
5967.6(5)	$1^\pm$	1.0	0.58(8)	7.8(11)	1.1(2)
5981.2(3)	$1^\pm$	1.0	1.11(14)	14.8(19)	0.59(8)
5998.3(8)[j]	$(1^\pm, 2^+)$	1.0	0.18(12)	2.3(16)	3.7(25)
6008.7(7)	$1^\pm$	1.0	0.32(6)	4.2(8)	2.1(4)
6020.1(6)[k]	$1^\pm$	1.0	0.46(23)	6.1(30)	1.4(7)
6054.0(15)	$1^\pm$	1.0	0.24(7)	3.1(9)	2.7(8)
6066.8(8)	$1^\pm$	1.0	0.31(8)	4.2(11)	2.1(5)
6074.2(11)	$1^\pm$	1.0	0.28(8)	3.6(10)	2.3(6)
6084.4(8)	$(1^\pm, 2^+)$	1.0	0.30(8)	3.8(10)	2.1(6)
6105.0(20)[l]	$(1^\pm, 2^+)$	$0.32^{+0.21}_{-0.14}$[m]	0.20(14)	8.06(536)	0.33(22)
6148.3(5)	$1^\pm$	1.0	0.49(12)	6.1(15)	1.3(3)
6161.2(6)	$(1^\pm, 2^+)$	1.0	0.43(12)	5.2(15)	1.5(4)
6194.4(8)[n]	$1^\pm$	1.0	0.27(16)	3.3(19)	2.4(15)
6210.0(6)[o]	$(1^\pm, 2^+)$	1.0	0.28(17)	3.3(21)	2.3(15)
6229.1(20)	$(1^\pm, 2^+)$	1.0	0.32(9)	3.9(10)	2.0(6)
6254.3(6)[p]	$1^\pm$	1.0	0.46(10)	5.4(11)	1.4(3)
6277.0(9)	$1^\pm$	1.0[q]	0.35(11)	4.1(13)	1.9(6)

(*continued*)

Table 6 (*Continued*)

E_x (keV)	J^π ($\hbar$)	Γ_0/Γ	Γ_0^2/Γ (eV)	$B(\sigma\lambda)\uparrow$ ([a])	τ (fs)
6322.9(5)	$1^\pm$	1.0	0.96(23)	10.9(26)	0.69(17)
6410.9(6)[r]	$1^\pm$	1.0	0.48(21)	5.2(23)	1.38(61)
6419.6(11)[r]	$(1^\pm, 2^+)$	1.0	0.22(13)	2.4(14)	3.02(175)
6456.9(9)	$(1^\pm, 2^+)$	1.0	0.41(17)	4.3(19)	1.6(7)
6469.3(7)[r]	$(1^\pm, 2^+)$	1.0	0.38(20)	4.0(21)	1.73(90)

[a] E1 strength in $10^{-3}\ e^2\ \mathrm{fm}^2$, M1 strength in μ_N^2, E2 strength in $e^2\ \mathrm{fm}^4$.

[b] Contribution of a decay branch from ^{206}Pb subtracted ($\sim$ 20%).

[c] Contribution of a decay branch from ^{206}Pb subtracted ($\sim$ 30%).

[d] Contribution from ^{207}Pb subtracted ($\sim$ 30%).

[e] Contribution of a single-escape peak subtracted ($\sim$ 40%).

[f] Possible decay branch coincides with a single-escape peak.

[g] Possible decay branch coindices with a single-escape peak of ^{206}Pb.

[h] Contribution from single-escape subtracted ($\sim$ 30%).

[i] Contribution from ^{208}Pb subtracted ($\sim$ 20%).

[j] Contributions from ^{206}Pb and from an escape peak of a transition in ^{207}Pb subtracted ($\sim$ 50% in total).

[k] Contributions from a transition in ^{206}Pb subtracted ($\sim$ 30%).

[l] Possible contribution from a transition in ^{206}Pb neglegted ($<$ 10%).

[m] Decay branch to the 2_1^+ state coincides with single-escape peak of another transition; contribution subtracted ($\sim$ 25%).

[n] Contribution from a transition in ^{208}Pb subtracted ($\sim$ 20%).

[o] Contribution from a single-escape peak of a transition in ^{208}Pb subtracted ($\sim$ 40%).

[p] Contribution from a transition in ^{208}Pb neglected ($<$ 10%).

[q] Possible decay branch coincides with a transition in ^{206}Pb.

[r] Assignment to ^{204}Pb unclear; peak coincides probably with a transition in ^{206}Pb; contribution subtracted ($\sim$ 25%).

$J = 3/2$. The distribution associated with an intermediate state of $J = 1/2$ is completely isotropic. For transitions with very small experimental uncertainties it is possible to estimate the multipole mixing parameter. Since the present experiment was not optimized for such a purpose, this was possible—with limited accuracy—for the example of the 4104 keV transition only (dotted curve). (We use here the phase convention by Biedenharn and Rose [63] which agrees with the Krane–Steffen phase convention [64] used in the nuclear data sheets for the decay of the excited states.)

Table 7 summarizes the experimental results. The listed values represent an error-weighted average of the two measurements with the targets with main components ^{206}Pb and ^{204}Pb, respectively. The results are compared to values from previous experiments in Table 8 with generally good agreement. Nevertheless, the experimental uncertainties for ^{207}Pb comparable to previous, dedicated experiments underline the high sensitivity of the setup presented in this paper.

The state at 3.3 MeV is obviously fed from higher-lying levels. Transitions previously assigned to ^{207}Pb at 4627 keV [48] and 5209 and 5233 keV [47] that have not been observed in Ref. [46] have not been detected in this experiment, either. Chapuran et al. [46] discuss a possible transition to the first excited $J^\pi = 5/2^-$ state from the 6181 keV level. This could not be studied in the present experiment due to the strong 5616 keV excitation in ^{206}Pb. The detected weak decay branch of the 5490 keV state into the first

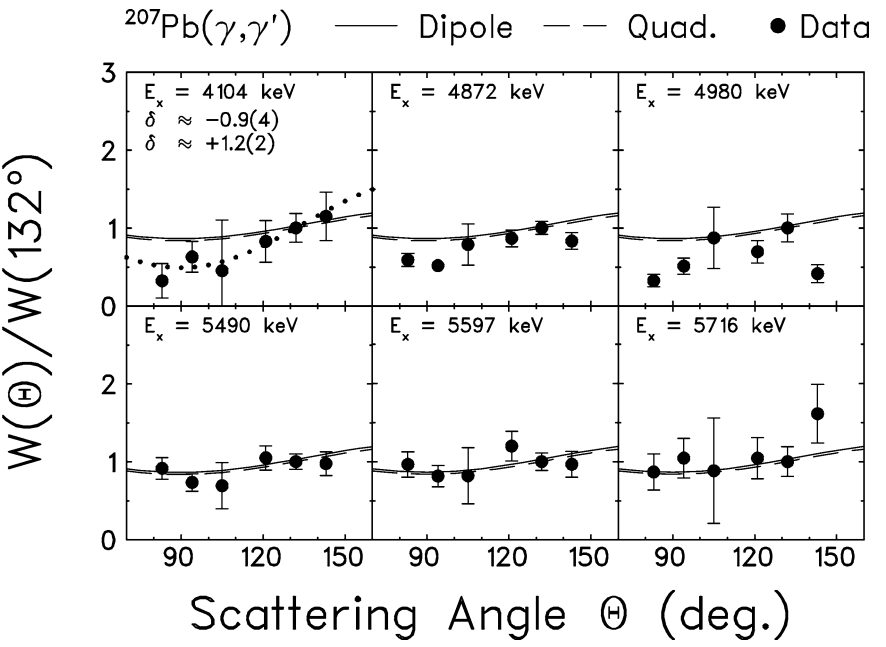

Fig. 11. Angular distribution ratios $W(\Theta)/W(132°)$ of transitions into the ground state of ^{207}Pb for the six effective scattering angles of the individual crystals of the two cluster detectors. The data have been extracted from the measurement of the mixed target with main component ^{206}Pb. The distributions have been normalized to the value at $\Theta = 132°$. The full and dashed lines indicate the theoretical distributions for dipole and quadrupole excitations, respectively. The curves show the expected distribution of a $(1/2 \to 3/2 \to 1/2)$ cascade. The distribution of the sequence $(1/2 \to 1/2 \to 1/2)$ is isotropic and not displayed in the figure. The dotted line for the 4104 keV excitation shows a fit to the experimental data with the quoted multipole mixing parameter δ.

excited $J^\pi = 5/2^-$ state at 570 keV basically excludes an $J^\pi = 1/2^+$ assignment. For the excitation at 6181 keV a larger transition strength was extracted than in previous studies [46]. This excludes the possibility that the transition is a decay branch of a level at 6749 keV which was not populated in the present experiment.

3.5. E1 strength distributions in ^{204,206,208}Pb

In this section, we will focus on the description of the E1 strength distribution in the even-mass isotopes ^{204,206,208}Pb. Some aspects have been discussed already within a previous publication [34]. The electromagnetic response of the odd-mass nucleus ^{207}Pb will be discussed later.

The top panel of Fig. 12 shows the extracted electric dipole strength distributions for ^{204,206,208}Pb. There are unambiguous assignments of the multipolarity for all excitations in ^{208}Pb. For ^{206}Pb electric character was assumed for all dipole excitations excluding a known 'isoscalar' M1 excitation that is discussed in the following section. In the isotope ^{204}Pb for all excited states where $J = 1$ could not be explicitly excluded, $J^\pi = 1^-$ has been assumed. A possible existence of an 'isoscalar' M1 excitation also in ^{204}Pb with a

Table 7
Results of the ^{207}Pb(γ,γ') experiment. Given are the excitation energy E_x, angular momentum and parity J^π, branching ratio Γ_0/Γ, $g\Gamma_0^2/\Gamma$ (proportional to the energy-integrated cross section), the reduced dipole transition width $g\Gamma_0^{\rm red}$, and, where applicable, the value of the multipole mixing parameter δ as obtained from the measured angular distribution. The lifetime τ is given, too. For determining transition widths and strengths, angular momentum values and mixing parameters were used in the angular distribution, but M1 and E2 contributions have not been separated. An isotropic angular distribution and $g = 1$ was assumed for exitations with unknown multipolarity and δ

E_x (keV)	J^π ($\hbar$)	Γ_0/Γ	$g\Gamma_0^2/\Gamma$ (eV)	$g\Gamma_0^{\rm red}$ $\left(\mathrm{meV/MeV^3}\right)$	δ	τ (fs)
3305.2(10)[a]	$\frac{1}{2}^+$	1.0	< 0.18	< 5		> 3.7
3928.9(10)[b]	$\frac{3}{2}^-$	1.0	0.43(33)	7.1(54)	$^{-0.10}_{+0.72}$[c]	1.53(117)
4103.8(5)	$\frac{3}{2}^-$	1.0	1.39(12)	20.2(17)	$^{-0.9(4)}_{+1.2(2)}$	0.47(4)
4140.7(5)	$\left(\frac{5}{2}\right)^-$	1.0	1.31(21)	18.5(30)[d]		0.50(8)
4871.6(3)	$\frac{1}{2}^\pm, \frac{3}{2}^\pm$	1.0	5.98(69)	51.7(60)		0.11(1)
4980.4(3)[e]	$\frac{1}{2}^+$	1.0	5.38(78)	43.6(63)		0.12(1)
5489.7(3)[f]	$\frac{1}{2}^-, \frac{3}{2}^\pm$	$0.84^{+0.16}_{-0.22}$	11.57(139)	70.0(84)	[g]	0.057(7)
5597.4(3)	$\frac{1}{2}^\pm, \frac{3}{2}^\pm$	1.0	12.09(141)	68.9(80)		0.054(6)
5690.0(16)[h]	$\frac{1}{2}^\pm, \frac{3}{2}^\pm$	1.0	1.97(135)	10.7(73)		0.33(23)
5715.6(4)	$\frac{1}{2}^\pm, \frac{3}{2}^\pm$	1.0	7.77(112)	41.6(60)		0.085(12)
6181.0(7)[i]	$\frac{1}{2}^\pm, \frac{3}{2}^\pm$	1.0[j]	5.93(119)	25.1(50)		0.111(22)

[a] Only observed in the experiment with main target component ^{206}Pb, contribution of a double-escape peak subtracted ($\sim 50\%$).

[b] Only observed in the experiment with main target component ^{206}Pb, contributions from single-escape peaks subtracted ($\sim 20\%$).

[c] From [48].

[d] Value corresponds to $B(\mathrm{E2})\uparrow = 1416(122)\ e^2\,\mathrm{fm}^4$.

[e] Analysis was only possible for the experiment with main target component ^{206}Pb.

[f] Decay branch to the first excited state coincides with single-escape peak of a transition in ^{204}Pb; the values given here were deduced from the experiment with main target component ^{206}Pb.

[g] The angular distribution from the experiment with main target component ^{204}Pb suggests $\delta = -1.3(2)$ or $\delta = 0.8(2)$, whereas from the experiment with main target component ^{206}Pb a nearly isotropic distribution is found. We use here $\delta = 0$ and $W(\Theta) = 1$.

[h] Transition coincides with a transition in ^{204}Pb; the values given here have been deduced from the measurement with main target component ^{206}Pb only; the contribution of a single-escape peak has been subtracted ($\sim 30\%$).

[i] Transition coincides with a transition in ^{204}Pb; the values given here have been deduced from the measurement with main target component ^{206}Pb only.

[j] Possible decay branch to the first excited state coincides with a transition in ^{206}Pb.

total strength of $B(\mathrm{M1})\uparrow \approx 2\ \mu_N^2$ must be considered (see below). However, if such M1 strength was erroneously assigned as E1 (corresponding to $B(\mathrm{E1})\uparrow \approx 20 \times 10^{-3}\ e^2\,\mathrm{fm}^2$ in the plot) it would not affect the conclusions on the gross properties of the strength distributions discussed below.

Table 8
Comparison of results of nuclear resonance fluorescence experiments on ^{207}Pb. Only the previously measured transitions that are listed in Table 7 are given

E_x (keV)	$g\Gamma_0^2/\Gamma^1$ (eV)	$g\Gamma_0^2/\Gamma^b$ (eV)	$g\Gamma_0^2/\Gamma^c$ (eV)	$g\Gamma_0^2/\Gamma^d$ (eV)	$g\Gamma_0^2/\Gamma^e$ (eV)
3305	< 0.18			0.04(1)	0.05(1)
3929	0.43(33)			0.68(8)	0.59(4)
4104	1.39(12)			1.10(12)	
4141	1.31(21)			1.38(18)	
4872	5.98(69)	7.1(11)	13[f]	3.6(5)	
4980	5.38(78)	6.1(12)	7[f]	4.0(5)	
5490	11.57(139)	11.4(19)	12[f]		
5597	12.09(141)	9.0(14)	8[f]		
5690	1.97(135)	3.0(6)			
5716	7.77(112)	6.2(12)	3[f]		
6181	5.93(119)	3.3(7)			

[a] This paper.
[b] Ref. [46].
[c] Ref. [47].
[d] Ref. [48].
[e] Ref. [61].
[f] Uncertainty in excess of 50% quoted.

In ^{204,206}Pb E1 strength is also detected at energies below 4 MeV. From systematics and model calculations it is reasonable to assume that the excitations below 4 MeV arise from the coupling of the quadrupole and octupole vibrations.

In all three nuclei, two E1 strength concentrations are visible around 5 and 6 MeV. One observes for the E1 strength in this energy region an increasing fragmentation when going from the closed-shell ^{208}Pb to ^{206}Pb and ^{204}Pb. The summed E1 strength in ^{208}Pb amounts to $\sum B(\mathrm{E1})\uparrow = 0.944(76)\ e^2\,\mathrm{fm}^2$, distributed over 9 levels. For ^{206}Pb one finds 37 levels above 4 MeV with a total strength of $\sum B(\mathrm{E1})\uparrow = 0.391(67)\ e^2\,\mathrm{fm}^2$, and in ^{204}Pb 40 levels carry $\sum B(\mathrm{E1})\uparrow = 0.235(73)\ e^2\,\mathrm{fm}^2$. The energy-weighted isovector electric dipole sum rule (EWSR) is exhausted by 0.705(58)% for ^{208}Pb, by 0.300(52)% for ^{206}Pb, and by 0.193(59)% for the case of ^{204}Pb due to the strengths detected below 6.75 MeV. In the present experiment, an increase of the experimental sensitivity by more than an order of magnitude has been achieved with respect to previous work (e.g., [46,52]) for ^{206,208}Pb.

For the case of ^{208}Pb, information from other spectroscopic probes is available. Alpha scattering, proton scattering, and transfer reactions [62,65–67] lead to no uniform picture for all E1 excitations below 7 MeV. The excitations appear to have dominantly isoscalar nature. Some are predicted to be collective, whereas others appear to have a rather pure 1p–1h structure, the 6.26 MeV state might even be a fragment of a spin-dipole mode. Such additional information is sparse for ^{206}Pb and does not exist for ^{204}Pb.

One possible interpretation of the detected E1 strength might be that it forms the low-energy tail of the isovector giant dipole resonance (IVGDR). If one fits a Lorentzian to the IVGDR data from (γ,n) reactions [68], the extrapolation of the strength distribution can be compared to the data. This is done in Fig. 13 where the binned experimental results (hatched bars) are shown as well as the extrapolation of the IVGDR (solid curve). While

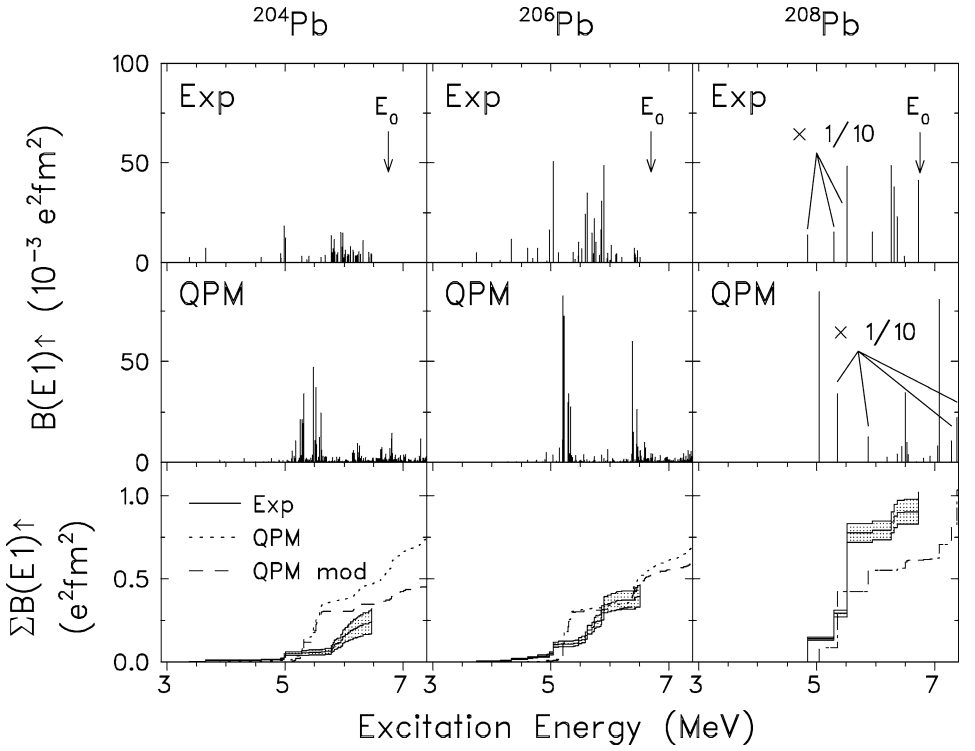

Fig. 12. Electric dipole strength distributions in ^{204,206,208}Pb (left to right). Top row: experimental strength distribution up to the endpoint energy of ~ 6.75 MeV (indicated by arrows). Middle row: predictions from the quasiparticle-phonon model (QPM). Bottom row: running sums from the experiment (solid histogram) and the QPM (dotted histogram). The dashed histogram shows the QPM prediction including the experimental detection limit.

the experimental strength distribution is of the right order of magnitude for ^{204,206}Pb, the model clearly fails in describing the strength observed for ^{208}Pb as well as the differences between the three nuclei. The simple extrapolation of the IVGDR Lorentzian to the energy range considered here is not a good approximation, especially in nuclei at or near closed shells. A far better description of the low-energy tail of the IVGDR can be obtained by using an energy-dependent width of the IVGDR as suggested in Ref. [69]. However, this phenomenological description yields even lower electric dipole strength predictions as can be seen from the dashed curve in Fig. 13, significantly smaller than the experimental results. A similar effect is obtained by taking the dynamical deformation of the nucleus into account and introducing a dipole–quadrupole interaction term as proposed by [70] for average resonance-capture photon spectra. Also the dotted curves in Fig. 13, showing the results from this model, fail to account for the detected strengths. In Fig. 13 another feature of the measured strength distributions is visible: The strength shifts to lower energies with increasing mass. The present data are not sufficient to clarify if this is due to the variation in the mass number (e.g., $\propto A^{-1/3}$ as for the IVGDR) or due to a variation in the N/Z ratio.

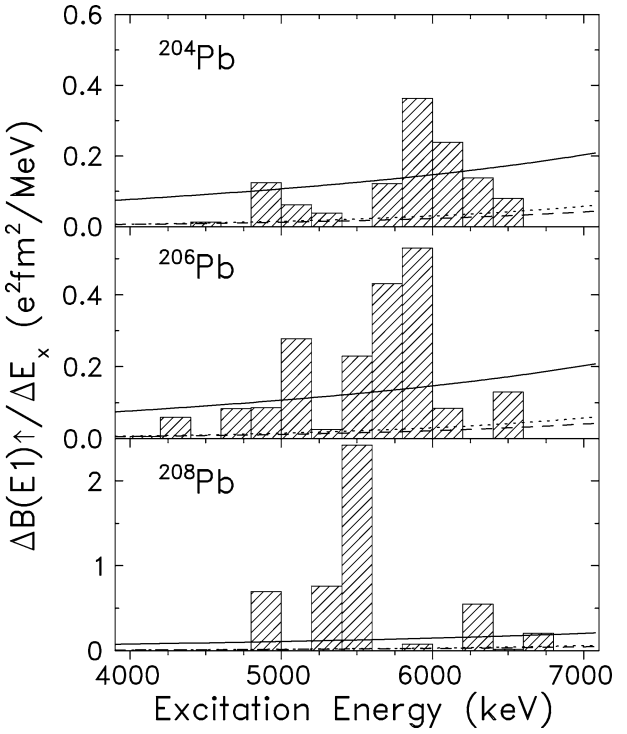

Fig. 13. Electric dipole strength distributions in ^{204,206,208}Pb compared with extrapolations of the isovector giant dipole resonance (IVGDR). For the description of the shape of the IVGDR a Lorentzian with constant width (full line), a Lorentzian with energy-dependent width (dotted line), and a Lorentzian with deformation dependent modifications (dashed line, see [70]) was assumed. Please note the different scales for the three nuclei.

The dependence of the excitation energy on the N/Z ratio is anticipated in models where a 'soft' dipole mode is predicted as a collective vibration of the excess neutrons with respect to a proton–neutron core. Such models have been around since the 1970s (see Section 1 for an overview over the literature). Calculations for ^{208}Pb within a hydrodynamical model [9] predict the centroid of the soft mode around 4.5 MeV with roughly a third of the strength measured in the experiment between 4 and 6.75 MeV. A theoretical study [13] within the random phase approximation (RPA) for ^{208}Pb predicts the soft mode around 9 MeV with a total strength comparable to the summed strength up to 6.75 MeV.

A more detailed understanding of the measured E1 strength can be obtained by comparing the experimental results with predictions of the microscopic quasiparticle-phonon nuclear model (QPM, see [29,30] and references therein for theoretical background information). Phonons with $J^\pi = 0^\pm$ to $6^\pm$ have been taken into account, and all possible two- and three-phonon configurations have been calculated up to an energy of 8.5 MeV to achieve a realistic description of the strength distributions up to about 8 MeV. In the present calculations we have used a single-particle basis from [32] which has been adjusted to a better reproduction of the E1 strength distribution below the threshold in ^{208}Pb. In this,

the present calculations go beyond the ones presented in our preceding letter [34]. The theoretical results are displayed in the middle panel of Fig. 12. They agree quantitatively to within a factor of two with the experimental strength distributions depicted in the top row. This is even more visible if one compares the running summed strength distributions as done in the lower part of Fig. 12. The solid histograms show the measured data, including a band for the experimental uncertainties. The QPM results are shown as a dashed histogram. To compare experiment and model prediction, an average experimental detection threshold was applied to the results from the model, resulting in the short-dashed histogram. The fragmentation with the opening of the neutron shell is well reproduced. For ^{204}Pb it is in fact probably even stronger than predicted within the QPM. With the opening of the neutron shell, the energies of the two-phonon states drop significantly, and the fragmentation with respect to ^{208}Pb increases. The energy shift of the centroid of the E1 strength observed experimentally, however, is not reproduced by the calculations. While the total predicted E1 strength and the number of expected states in ^{204,206}Pb agrees well with theory—imposing the experimental detection threshold on the model predictions—too little strength is predicted in the energy interval below 7 MeV for ^{208}Pb.

More recently, new photon scattering results on ^{208}Pb at and above the neutron threshold have found more dipole strength [32]. If one averages over the predicted charge transition densities of all E1 excitations up to 8 MeV, one finds from the QPM evidence for an oscillation of the excess neutrons with respect to a proton–neutron 'core' and toroidal modes [22–24]. Direct experimental evidence for the structure of the states around 8 MeV is still lacking, especially about possible mixing between neutron-skin oscillations, toroidal modes, the IVGDR, and low-lying 1p–1h excitations. One possibility to study the structure of the excitation is measuring form factors in electron scattering at low momentum transfer.

The predicted neutron-skin oscillation is especially visible when plotting the radial charge transition densities $r^2_{\mathrm{p/n}}\rho_{\mathrm{p/n}}(r)$ for protons and neutrons separately as a function of the distance from the center of the nucleus. This is shown in Fig. 14 for ^{204}Pb (top), ^{206}Pb, and ^{208}Pb (bottom), displaying neutron densities as solid lines and proton densities as dashed lines. As in Ref. [32], the densities shown here have been obtained by summing the charge transition densities of all E1 excitations up to 8 MeV; weak excitations therefore contribute less than strong ones. One recognizes that neutrons on the outer part of the nucleus contribute as does an in-phase motion of protons and neutrons about 5 fm from the center. The pattern is rather similar for all three isotopes considered. This suggests that the QPM expects a collective neutron-skin vibration in the Pb isotopes.

3.6. Other multipolarities

For most of the states in ^{204,206}Pb a parity assignment is not possible. To elucidate possible M1 contributions, we discuss the predicted M1 strength within a shell-model approach [71] including two- and four-hole excitations with respect to the ^{208}Pb core, see, e.g., [72]. The configuration space includes the orbitals $2p_{1/2}$, $1f_{5/2}$, $2p_{3/2}$, $0i_{13/2}$, $1f_{7/2}$, and $0h_{9/2}$, and single-particle energies have been extracted from the low-energy spectrum of ^{207}Pb. The interaction is based on a Bonn-A potential using a G-matrix formalism.

For ^{206}Pb four M1 excitations below 7 MeV are predicted. The well-known 1^+ state at 1.7 MeV is nicely reproduced [73]. With the exception of an expected, but yet

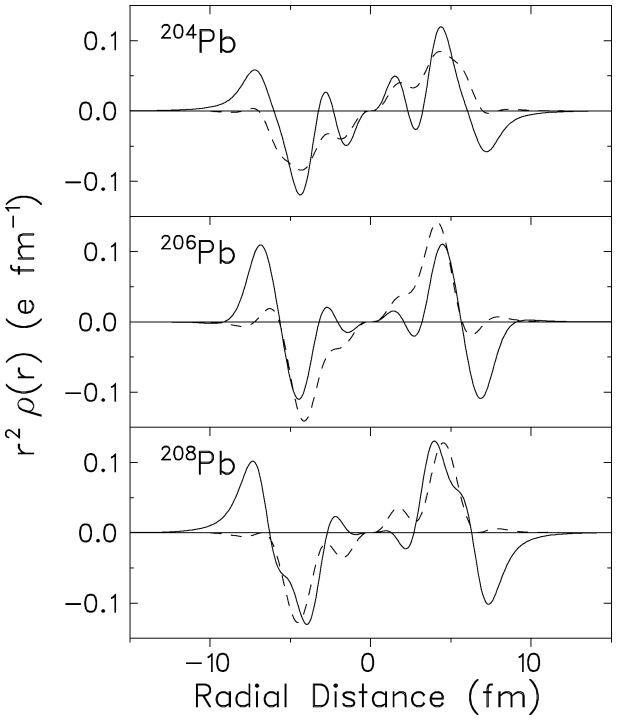

Fig. 14. Transition charge densities for E1 excitations for protons (dashed curves) and neutrons (solid curves) from the quasiparticle-phonon model for ^{204}Pb (top), ^{206}Pb (middle), and ^{208}Pb (bottom). The transition densities have been averaged over states up to 8 MeV excitation energy; in ^{208}Pb, the lowest E1 excitation, which is a pure neutron excitation, has been left out. The excess neutron vibration already discussed in Ref. [32] is clearly visible in all three isotopes, although the pattern for ^{204}Pb is a little more washed out.

unidentified $f_{5/2}^{-1}f_{7/2}^{-1}$ state around 3.9 MeV with $B(\mathrm{M1}) = 0.15\ \mu_N^2$, the higher-lying M1 excitations are below the detection limit of the present experiment. Since the present model space excludes core excitations, it does not describe the M1 strength at high energies appropriately. The most prominent example is an M1 mode around 5.8 MeV with proton–neutron symmetry in the wave function which is usually referred to as 'isoscalar', see [74–76] and references therein. For experimental results on the M1 excitation strength above 6.7 MeV, we refer to [77,78].

The number of predicted M1 excitations in ^{204}Pb is much larger; about 90 states are expected to exist below 7 MeV, 33 of which are below 4 MeV. Although a detailed calculation of the M1 strength does not exist at the moment, it is clear that there is no additional strength with respect to ^{206}Pb, but rather a fragmentation. The higher density of 1^+ levels in ^{204}Pb around 5.8 MeV might lead to a fragmentation of 'isoscalar' M1 strength, as well.

Relatively few E2 excitations have been observed in the present experiment. The excitation and decay of 2^+ states in ^{208}Pb is particularly interesting because of the open question of two-octupole-phonon states in this nucleus. A discussion of this topic including

the results from the present work has been published elsewhere [33]. In ^{204,206}Pb, E2 excitations have been found around 4.1 MeV, close to the energy of the core-quadrupole excitation in ^{208}Pb at 4085 keV. The total strength associated with the E2 excitations in the open-shell nuclei is much smaller than in ^{208}Pb.

3.7. Electromagnetic response of ^{207}Pb

The results obtained for ^{207}Pb are consistent with previous findings so that the conclusions drawn from previous work, e.g., [46], remain unchanged. Consequently it is still not understood why the dipole strength distribution in ^{207}Pb cannot be described by the weak coupling of a neutron-$p_{1/2}$ hole to the excitations in ^{208}Pb. The summed E1 strength up to 6.7 MeV—assuming E1 character for all excitations above 4.5 MeV—corresponds instead to the E1 strength in ^{206}Pb.

To improve our understanding of the E1 strength in ^{207}Pb, QPM calculations have been performed with the model presented in [79] for the Sn region. Three-phonon configurations could not be included due to the huge number of configurations involved for an odd-mass nucleus. This leads to near-degeneracies of the calculated eigen energies and to an underestimation of the degree of fragmentation.

Fig. 15 shows the experimental distribution of the energy-integrated photon scattering cross sections into the g.s. ($I_f = I_0$ in Eq. (2)) in the top panel, the QPM predictions in the middle panel, and the comparison of the running sums in the bottom panel (solid histogram for experimental data, dashed histogram for QPM prediction, and short-dashed histogram for the QPM results convoluted with an empirical average detection threshold).

Note that the plotted integrated scattering cross sections are from E1, M1, and E2 transitions. From the QPM calculations, only one E2 excitation around 4 MeV contributes significantly, and about half of the states around 6.2 MeV are due to M1 excitations; the rest is electric dipole strength. The QPM predicts similar strengths for ^{207}Pb and ^{208}Pb, contrary to the experimental data.

4. Concluding remarks

In summary, we have performed high-resolution nuclear resonance fluorescence experiments with unprecedented sensitivity on ^{204,206,207,208}Pb. Dipole and electric quadrupole excitations have been extracted. The experimental results have been compared to new QPM calculations, and overall agreement has been found. The QPM results are capable of accounting for the fragmentation of the electric dipole strength, but are not conclusive for the understanding of the shift of the centroid of the distribution in the even-mass nuclei or the reduced overall strength in the odd-mass nucleus ^{207}Pb.

The results of various experiments and phenomenological models suggest that the E1 strength below 7 MeV is not due to an out-of-phase oscillation of excess neutrons versus an $N \approx Z$ core. The QPM predictions also show varying configurations for the lowest state, but a neutron-skin vibration is predicted for all Pb isotopes at energies around 8 MeV. Indirect evidence for such a mode has been identified recently from a photon scattering experiment up to 9 MeV in ^{208}Pb in comparison with QPM calculations [32]. However, direct evidence on the structure of these states at or above the neutron separation threshold is still missing.

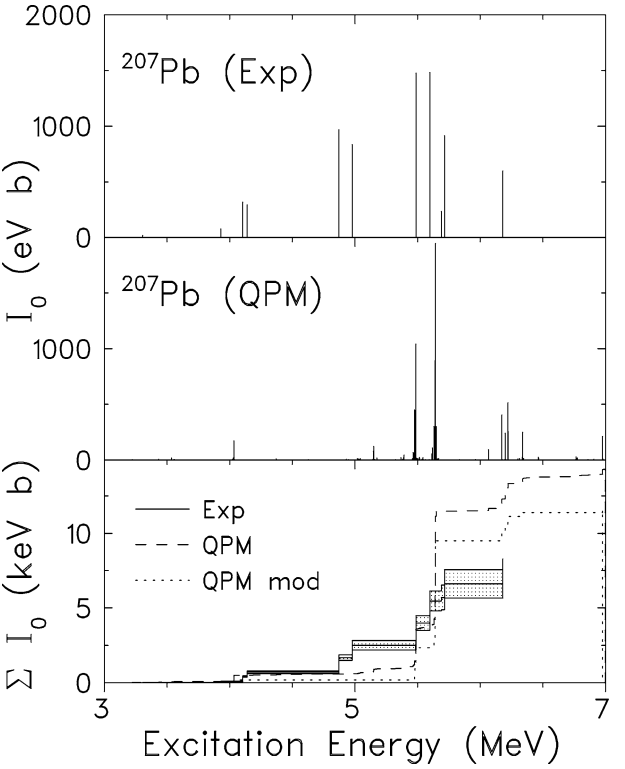

Fig. 15. Energy-integrated scattering cross section of excitations in the odd-mass nucleus ^{207}Pb. Top panel: experimental distribution. Middle panel: predictions within the quasiparticle-phonon model (QPM). Bottom panel: running sums of the experimental distribution (solid histogram) and the QPM (dashed histogram). The short-dashed histogram shows the QPM prediction including an estimated experimental detection threshold.

Acknowledgements

We are indebted to H. Prade, H. Schnare, S. Skoda, H.G. Thomas, H. Tiesler, and D. Weisshaar for their support during the experiment. We thank H.-D. Gräf and the S-DALINAC staff for the reliable operation of the accelerator and A. Gargano and colleagues for providing us with the shell-model calculations on the M1 strength distribution in ^{204,206}Pb. Discussions with U. Kneissl, P. Mohr, H.H. Pitz, and A. Zilges are gratefully acknowledged. We are indebted to R. Stock for the loan of the ^{206}Pb target.

References

[1] U. Kneissl, H.H. Pitz, A. Zilges, Prog. Part. Nucl. Phys. 37 (1996) 349.
[2] D. Bohle, A. Richter, W. Steffen, A.E.L. Dieperink, N. Lo Iudice, F. Palumbo, O. Scholten, Phys. Lett. B 137 (1984) 27.

[3] A. Linnemann, P. von Brentano, J. Eberth, J. Enders, A. Fitzler, C. Fransen, E. Guliyev, R.-D. Herzberg, L. Käubler, A.A. Kuliev, P. von Neumann-Cosel, N. Pietralla, H. Prade, A. Richter, R. Schwengner, H.G. Thomas, D. Weisshaar, I. Wiedenhöver, Phys. Lett. B 554 (2003) 15.
[4] A. Nord, J. Enders, A.E. de Almeida Pinto, D. Belic, P. von Brentano, C. Fransen, U. Kneissl, C. Kohstall, A. Linnemann, P. von Neumann-Cosel, H.H. Pitz, A. Richter, F. Stedile, V. Werner, Phys. Rev. C 67 (2003) 034307.
[5] D. Zawischa, J. Phys. G 24 (1998) 683.
[6] N. Lo Iudice, Riv. Nuovo Cimento 23 (2000) 1.
[7] K. Heyde, A. Richter, Rev. Mod. Phys., in preparation.
[8] G.A. Bartholomew, E.D. Earle, A.J. Ferguson, J.W. Knowles, M.A. Lone, Adv. Nucl. Phys. 7 (1972) 229.
[9] R. Mohan, M. Danos, L.C. Biedenharn, Phys. Rev. C 3 (1971) 1740.
[10] Y. Suzuki, K. Ikeda, H. Sato, Prog. Theor. Phys. 83 (1990) 180.
[11] P. Van Isacker, M.A. Nagarajan, D.D. Warner, Phys. Rev. C 45 (1992) R13.
[12] J. Chambers, E. Zaremba, J.P. Adams, B. Castel, Phys. Rev. C 50 (1994) R2671.
[13] J.P. Adams, B. Castel, H. Sagawa, Phys. Rev. C 53 (1996) 1016.
[14] S.I. Bastrukov, S. Misicu, A.V. Sushkov, Nucl. Phys. A 562 (1993) 191.
[15] E.B. Balbutsev, I.V. Molodtsova, A.V. Unzhakova, Europhys. Lett. 26 (1994) 499.
[16] S. Misicu, S.I. Bastrukov, Eur. Phys. J. A 13 (2002) 399.
[17] F. Iachello, Phys. Lett. B 160 (1985) 1.
[18] A.M. Oros, K. Heyde, C. De Coster, B. Decroix, Phys. Rev. C 57 (1998) 990.
[19] G. Colò, N. Van Giai, P.F. Bortignon, M.R. Quaglia, Phys. Lett. B 485 (2000) 362.
[20] D. Vretenar, A. Wandelt, P. Ring, Phys. Lett. B 487 (2000) 334.
[21] J. Piekarewicz, Phys. Rev. C 64 (2001) 024307.
[22] D. Vretenar, N. Paar, P. Ring, G.A. Lalazissis, Phys. Rev. C 63 (2001) 047301.
[23] D. Vretenar, N. Paar, P. Ring, T. Nikšić, Phys. Rev. C 65 (2002) 021301R.
[24] J. Kvasil, N. Lo Iudice, Ch. Stoyanov, P. Alexa, J. Phys. G 29 (2003) 753.
[25] A. Leistenschneider, T. Aumann, K. Boretzky, D. Cortina, J. Cub, U.D. Pramanik, W. Dostal, Th.W. Elze, H. Emling, H. Geissel, A. Grünschloss, M. Hellström, R. Holzmann, S. Ilievski, N. Iwasa, M. Kaspar, A. Kleinbohl, J.V. Kratz, R. Kulessa, Y. Leifels, E. Lubkiewicz, G. Münzenberg, P. Reiter, M. Rejmund, C. Scheidenberger, C. Schlegel, H. Simon, J. Stroth, K. Sümmerer, E. Wajda, W. Walus, S. Wan, Phys. Rev. Lett. 86 (2001) 5442.
[26] E. Tryggestad, T. Aumann, T. Baumann, D. Bazin, J.R. Beene, Y. Blumenfeld, B.A. Brown, M. Chartier, M.L. Halbert, P. Heckman, J.F. Liang, D.C. Radford, D. Shapira, M. Thoennessen, R.L. Varner, Phys. Lett. B 541 (2002) 52.
[27] P. Mohr, J. Enders, T. Hartmann, H. Kaiser, D. Schiesser, S. Schmitt, S. Volz, F. Wissel, A. Zilges, Nucl. Instrum. Methods Phys. Res. A 423 (1999) 480.
[28] T. Hartmann, J. Enders, P. Mohr, K. Vogt, S. Volz, A. Zilges, Phys. Rev. Lett. 85 (2000) 274;
T. Hartmann, J. Enders, P. Mohr, K. Vogt, S. Volz, A. Zilges, Phys. Rev. Lett. 86 (2001) 4981, Erratum;
T. Hartmann, J. Enders, P. Mohr, K. Vogt, S. Volz, A. Zilges, Phys. Rev. C 65 (2002) 034301.
[29] R.-D. Herzberg, P. von Brentano, J. Eberth, J. Enders, R. Fischer, N. Huxel, T. Klemme, P. von Neumann-Cosel, N. Nicolay, N. Pietralla, V.Yu. Ponomarev, J. Reif, A. Richter, C. Schlegel, R. Schwengner, S. Skoda, H.G. Thomas, I. Wiedenhöver, G. Winter, A. Zilges, Phys. Lett. B 390 (1997) 49.
[30] R.-D. Herzberg, C. Fransen, P. von Brentano, J. Eberth, J. Enders, A. Fitzler, L. Käubler, H. Kaiser, P. von Neumann-Cosel, N. Pietralla, V.Yu. Ponomarev, H. Prade, A. Richter, H. Schnare, R. Schwengner, S. Skoda, H.G. Thomas, H. Tiesler, D. Weisshaar, I. Wiedenhöver, Phys. Rev. C 60 (1999) 051307R.
[31] A. Zilges, S. Volz, M. Babilon, T. Hartmann, P. Mohr, K. Vogt, Phys. Lett. B 542 (2002) 43.
[32] N. Ryezayeva, T. Hartmann, Y. Kalmykov, H. Lenske, P. von Neumann-Cosel, Y.Yu. Ponomarev, A. Richter, A. Shevchenko, S. Volz, J. Wambach, Phys. Rev. Lett. 89 (2002) 272502.
[33] J. Enders, P. von Brentano, J. Eberth, A. Fitzler, C. Fransen, R.-D. Herzberg, H. Kaiser, L. Käubler, P. von Neumann-Cosel, N. Pietralla, V.Yu. Ponomarev, A. Richter, H. Schnare, R. Schwengner, S. Skoda, H.G. Thomas, H. Tiesler, D. Weisshaar, I. Wiedenhöver, Nucl. Phys. A 674 (2000) 3.
[34] J. Enders, P. von Brentano, J. Eberth, A. Fitzler, C. Fransen, R.-D. Herzberg, H. Kaiser, L. Käubler, P. von Neumann-Cosel, N. Pietralla, V.Yu. Ponomarev, H. Prade, A. Richter, H. Schnare, R. Schwengner, S. Skoda, H.G. Thomas, H. Tiesler, D. Weisshaar, I. Wiedenhöver, Phys. Lett. B 486 (2000) 279.

[35] F.R. Metzger, Prog. Nucl. Phys. 7 (1959) 53.
[36] A. Richter, in: S. Myers, et al. (Eds.), Proceedings Fifth European Particle Accelerator Conference, Sitges/Barcelona (1996), Institute of Physics Publishing, Bristol, 1996, p. 110.
[37] H. Kaiser, P. von Brentano, E. Caurier, J. Eberth, J. Enders, A. Fitzler, C. Fransen, R.-D. Herzberg, L. Käubler, P. von Neumann-Cosel, N. Pietralla, A. Poves, H. Prade, A. Richter, H. Schnare, R. Schwengner, S. Skoda, H.G. Thomas, H. Tiesler, D. Weisshaar, I. Wiedenhöver, Nucl. Phys. A 660 (1999) 41;
H. Kaiser, P. von Brentano, E. Caurier, J. Eberth, J. Enders, A. Fitzler, C. Fransen, R.-D. Herzberg, L. Käubler, P. von Neumann-Cosel, N. Pietralla, A. Poves, H. Prade, A. Richter, H. Schnare, R. Schwengner, S. Skoda, H.G. Thomas, H. Tiesler, D. Weisshaar, I. Wiedenhöver, Nucl. Phys. A 669 (2000) 368, Erratum;
H. Kaiser, P. von Brentano, E. Caurier, J. Eberth, J. Enders, A. Fitzler, C. Fransen, R.-D. Herzberg, L. Käubler, P. von Neumann-Cosel, N. Pietralla, A. Poves, H. Prade, A. Richter, H. Schnare, R. Schwengner, S. Skoda, H.G. Thomas, H. Tiesler, D. Weisshaar, I. Wiedenhöver, Nucl. Phys. A 679 (2001) 869, Erratum.
[38] J. Eberth, H.G. Thomas, D. Weisshaar, F. Becker, B. Fiedler, S. Skoda, P. von Brentano, C. Gund, L. Palafox, P. Reiter, D. Schwalm, D. Habs, T. Servene, R. Schwengner, H. Schnare, W. Schulze, H. Prade, G. Winter, A. Jungclaus, C. Lingk, C. Teich, K.P. Lieb, Prog. Part. Nucl. Phys. 38 (1997) 29.
[39] N. Pietralla, I. Bauske, O. Beck, P. von Brentano, W. Geiger, R.-D. Herzberg, U. Kneissl, J. Margraf, H. Maser, H.H. Pitz, A. Zilges, Phys. Rev. C 51 (1995) 1021.
[40] C. Hutter, M. Babilon, W. Bayer, D. Galaviz, T. Hartmann, P. Mohr, S. Müller, W. Rochow, D. Savran, K. Sonnabend, K. Vogt, S. Volz, A. Zilges, Nucl. Instrum. Methods Phys. Res. A 489 (2002) 247.
[41] D. Weisshaar, Diplomarbeit, Universität zu Köln, 1995, unpublished.
[42] N. Pietralla, H.R. Weller, V.N. Litvinenko, M.W. Ahmed, A.P. Tonchev, Nucl. Instrum. Methods Phys. Res. A 483 (2002) 556.
[43] N. Pietralla, Z. Berant, V.N. Litvinenko, F.F. Mikhailov, G. Swift, M.W. Ahmed, J.H. Kelley, S.O. Nelson, R. Prior, K. Sabourov, A.P. Tonchev, H.R. Weller, Phys. Rev. Lett. 88 (2002) 012502.
[44] N. Pietralla, V.N. Litvinenko, S. Hartman, F.F. Mikhailov, I.V. Pinayev, G. Swift, M.W. Ahmed, J.H. Kelley, S.O. Nelson, R. Prior, K. Sabourov, A.P. Tonchev, H.R. Weller, Phys. Rev. C 65 (2002) 047305;
N. Pietralla, V.N. Litvinenko, S. Hartman, F.F. Mikhailov, I.V. Pinayev, G. Swift, M.W. Ahmed, J.H. Kelley, S.O. Nelson, R. Prior, K. Sabourov, A.P. Tonchev, H.R. Weller, Phys. Rev. C 65 (2002) 069901, Erratum.
[45] M.J. Martin, Nucl. Data Sheets 47 (1986) 797;
Evaluated Experimental Nuclear Structure Data File, National Nuclear Data Center Brookhaven, NY, 1999.
[46] T. Chapuran, R. Vodhanel, M.K. Brussel, Phys. Rev. C 22 (1980) 1420.
[47] D.F. Coope, L.E. Cannell, M.K. Brussel, Phys. Rev. C 15 (1977) 1977.
[48] C.P. Swann, J. Franklin Inst. 298 (1974) 321.
[49] C.P. Swann, Phys. Rev. Lett. 32 (1974) 1449.
[50] J.W. Knowles, A.M. Khan, W.F. Mills, Can. J. Phys. 56 (1978) 1021.
[51] K. Ackermann, K. Bangert, U.E.P. Berg, G. Junghans, R.K.M. Schneider, R. Stock, K. Wienhard, Nucl. Phys. A 372 (1981) 1.
[52] K. Wienhard, K. Ackermann, K. Bangert, U.E.P. Berg, C. Bläsing, W. Naatz, A. Ruckelshausen, D. Rück, R.K.M. Schneider, R. Stock, Phys. Rev. Lett. 49 (1982) 18.
[53] R.M. Laszewski, P. Axel, Phys. Rev. C 19 (1979) 342.
[54] S. Müller, A. Richter, E. Spamer, W. Knüpfer, B.C. Metsch, Phys. Lett. B 120 (1983) 305;
S. Müller, A. Richter, E. Spamer, W. Knüpfer, B.C. Metsch, Phys. Lett. B 122 (1983) 488, Erratum.
[55] S. Müller, G. Küchler, A. Richter, H.P. Blok, H. Blok, C.W. de Jager, H. de Vries, J. Wambach, Phys. Rev. Lett. 54 (1985) 293.
[56] J. Enders, Dissertation D17, Technische Universität Darmstadt, 2000;
http://elib.tu-darmstadt.de/diss/000035/.
[57] R.G. Helmer, M.A. Lee, Nucl. Data Sheets 61 (1990) 93;
Evaluated Experimental Nuclear Structure Data File, National Nuclear Data Center Brookhaven, NY, 2003.
[58] J.K. Dickens, Phys. Rev. C 28 (1983) 916.
[59] W.A. Lanford, Phys. Rev. C 16 (1977) 988.
[60] M. Schanz, A. Richter, E. Lipparini, Phys. Rev. C 36 (1987) 555.
[61] A. Nord, S.W. Yates, O. Beck, D. Belic, P. von Brentano, T. Eckert, C. Fransen, R.-D. Herzberg, U. Kneissl, H. Maser, N. Pietralla, H.H. Pitz, V. Werner, Phys. Rev. C 57 (1998) 3459.
[62] H.P. Morsch, P. Decowski, W. Benenson, Nucl. Phys. A 297 (1978) 317.

[63] L.C. Biedenharn, M.E. Rose, Rev. Mod. Phys. 25 (1953) 729.
[64] K.S. Krane, R.M. Steffen, Phys. Rev. C 2 (1970) 724.
[65] T.D. Poelhekken, S.K.B. Hesmondhalgh, H.J. Hofmann, A. van der Woude, M.N. Harakeh, Phys. Lett. B 278 (1992) 423.
[66] E. Radermacher, M. Wilhelm, S. Albers, J. Eberth, N. Nicolay, H.G. Thomas, H. Tiesler, P. von Brentano, R. Schwengner, S. Skoda, G. Winter, K.H. Maier, Nucl. Phys. A 597 (1996) 408.
[67] M. Schramm, K.H. Maier, M. Rejmund, L.D. Wood, N. Roy, A. Kuhnert, A. Aprahamian, J. Becker, M. Brinkman, D.J. Decman, E.A. Henry, R. Hoff, D. Manatt, L.G. Mann, R.A. Meyer, W. Stoeffl, G.L. Struble, T.-F. Wang, Phys. Rev. C 56 (1997) 1320.
[68] S.L. Dietrich, B.L. Berman, At. Data Nucl. Data Tables 38 (1988) 199.
[69] J. Kopecky, M. Uhl, Phys. Rev. C 41 (1990) 1941.
[70] S.F. Mughabghab, C.L. Dunford, Phys. Lett. B 487 (2000) 155.
[71] A. Gargano, 1999, private communication.
[72] L. Coraggio, A. Covello, A. Gargano, N. Itaco, T.T.S. Kuo, Phys. Rev. C 58 (1998) 3346.
[73] F.R. Metzger, Ann. Phys. (N.Y.) 66 (1971) 697.
[74] E. Lipparini, A. Richter, Phys. Lett. B 144 (1984) 13.
[75] V.Yu. Ponomarev, A. Vdovin, C. Velchev, J. Phys. G 13 (1987) 1523.
[76] R. Ratzek, U.E.P. Berg, C. Bläsing, A. Jung, S. Schennach, R. Stock, F.-J. Urban, H. Wickert, Phys. Rev. Lett. 56 (1986) 568.
[77] R.M. Laszewski, P. Rullhusen, S.D. Hoblit, S.F. LeBrun, Phys. Rev. Lett. 54 (1985) 530.
[78] H. Ohgaki, H. Toyokawa, T. Noguchi, S. Sugiyama, T. Mikado, K. Yamada, R. Suzuki, T. Ohdaira, N. Sei, T. Yamazaki, Nucl. Phys. A 649 (1999) 73c.
[79] V.Yu. Ponomarev, J. Bryssinck, L. Govor, F. Bauwens, O. Beck, D. Belic, P. von Brentano, D. De Frenne, C. Fransen, R.-D. Herzberg, E. Jacobs, U. Kneissl, H. Maser, A. Nord, N. Pietralla, H.H. Pitz, V. Werner, Phys. Rev. Lett. 83 (1999) 4029.